MODELLING AND CONTROL OF A SYMMETRIC FLAPPING WING VEHICLE: AN OPTIMAL CONTROL APPROACH

A Thesis

by

JUSTIN PATRICK JACKSON

Submitted to the Office of Graduate Studies of
Texas A&M University
in partial fulfillment of the requirements for the degree of

MASTER OF SCIENCE

August 2008

Major Subject: Aerospace Engineering

MODELLING AND CONTROL OF A SYMMETRIC FLAPPING WING VEHICLE: AN OPTIMAL CONTROL APPROACH

A Thesis

by

JUSTIN PATRICK JACKSON

Submitted to the Office of Graduate Studies of
Texas A&M University
in partial fulfillment of the requirements for the degree of

MASTER OF SCIENCE

Approved by:

Chair of Committee,	Thomas Strganac
Committee Members,	Johnny Hurtado
	Raktim Bhattacharya
	John Sweetman
Head of Department,	Helen Reed

August 2008

Major Subject: Aerospace Engineering

ABSTRACT

Modelling and Control of a Symmetric Flapping Wing
Vehicle: An Optimal Control Approach. (August 2008)
Justin Patrick Jackson, B.S., Texas A&M University at Galveston
Chair of Advisory Committee: Dr. Thomas Strganac

This thesis presents a method for designing a flapping wing stroke for a flapping wing vehicle. A flapping wing vehicle is a vehicle such as a bird or an insect that uses its wings for propulsion instead of a conventional propeller or a jet engine. The intent of this research is to design a wing stroke that the wings can follow which will maintain the vehicle at a desired longitudinal flight path angle and velocity. The cost function is primarily a function of the flight path angle error, velocity error and control rate. The objective maneuver is to achieve a flight condition similar to the trim of a conventional fixed wing aircraft. Gliding configurations of the vehicle are analyzed to better understand flight in minimal energy configurations as well as the modes of the vehicle. A control law is also designed using Lyapunov's direct method that achieves stable tracking of the wing stroke. Results are presented that demonstrate the ability of the method to design wing strokes that can maintain the vehicle at various flight path angles and velocities. The results of this research show that an optimal control problem can be posed such that the solution of the problem results in a wing stroke that a flapping wing vehicle can use to achieve a desired maneuver. The vehicle velocity is shown to be stable in controlled gliding flight and flapping flight.

To Dorothy

ACKNOWLEDGMENTS

Special thanks to Dr. Thomas Strganac for helping me into the Aerospace engineering program at Texas A&M, for encouraging my inspirations and for giving me a remarkable amount of freedom to pursue my ideas. Thanks to Dr. Bert Sweetman for encouraging my development starting when I was a sophomore and helping me down the academic road to graduate school. I am thankful for the zeal of Dr. John Hurtado and for teaching scintillating dynamics courses and spreading his interest to me. Thanks to Dr. Raktim Bhattacharya for encouraging this research and helping me to ask better questions of my work. And to Mrs. Karen Kanabe for guiding me through the occasional administrative hiccup. Also thanks to the TAMU LSAMP program for the financial assistance that has contributed to my academic freedom.

Thanks to Ashivni Shekhawat for illuminating many mathematical shortcomings and for assisting my growth as a questioning engineer. To James Doebbler for being interested in so many things, including my work and for endlessly offering his useful perspective. And to all of my other peers in the department who have encouraged my growth as a person and as an engineer throughout my master's program.

Thank you to all of my parents. My mother and stepfather, Kimiko and Jim, my father and stepmother, Kenneth and Patricia, for continuing to believe that I am smarter than I think I am and for supporting my directions in life. And lastly, my grandmother, who will always be a model of grace and tenacity for me to look up to.

TABLE OF CONTENTS

CHAPTER Page

LIST OF TABLES

LIST OF FIGURES

FIGURE Page

FIGURE Page

FIGURE Page

CHAPTER I

INTRODUCTION

The flapping wing problem has received much attention in recent years. The wings of these vehicles must provide lift to counteract gravity and thrust to counteract drag. These vehicles have the potential to excel in areas of maneuverability and silent flight which makes this prospect one of interest for operation in restricted spaces and surveillance applications. There are many issues that must be dealt with when attempting to characterize the dynamics of these vehicles because they are complex multi-body systems. The aerodynamics of these vehicles is also difficult to characterize. Phenomena such as wing leading edge vortices play an important role in lift production [1]. The control of flapping wing vehicles is another difficult problem. One question associated with controlling vehicles of this type is, how should the wings be moved in order to achieve a desired maneuver? A method of designing a flapping wing stroke for a flapping wing vehicle is presented here. The formulation includes a new model for a vehicle with two wings. This method takes an optimal control approach to designing the wing stroke. Perspectives on feedback control of the vehicle in gliding flight and flapping flight are presented. A stability analysis of the system in various flight configurations is also presented.

Researchers have investigated aspects of the flapping wing problem from various points of view. The complex motions of flapping wings through a fluid have been studied extensively [2, 3, 4, 5, 6, 7, 8, 9, 10]. The importance of the leading edge

---

This journal model is *IEEE Transactions on Automatic Control*.

vortex on lift production in flapping wing systems has also been investigated [1, 11, 12, 13, 9]. Some researchers use vortex panel methods to model the complex flows around flapping wings [10, 7, 4]. Here, a quasi-steady approach common to aircraft flight dynamics is used [14, 15] in the interest of the efficiency of the optimization routine. However, this quasi-steady aerodynamic model has limitations, these are discussed in Chapter V.

The dynamics of flapping wing vehicles are complex. These are multi-body systems with constraints dictating the permissible motions of the system. Researchers [2, 7, 16, 17, 18, 19, 20] have made simplifications in order to study specific aspects of a system such as flight path control and wing stroke design and some have taken a general approach to the development of the dynamic equations [20, 19, 17].

Inherent in controlling a flapping wing vehicle is the guidance and control of the wings of the vehicle. The wings must achieve motions that effectively manipulate the aerodynamics. The resulting aerodynamic forces will provide the lift and thrust that the vehicle requires for maneuvering. The problem of optimization of the wings' trajectories subject to the various constraints has also been studied [2, 3]. This thesis discusses the optimal control problem of guiding the wings of the vehicle in detail in Chapter VI. The tracking of a wing stroke has been addressed by others [19, 20, 18, 17, 7] and is also addressed in detail in this thesis.

A general perspective on some current issues facing researchers and designers of flapping wing vehicles is presented in [21]. Problems such as scaling issues arise when considering radio communication and the maximum size of antenna. Other more apparent topics such as stored energy, for which there is no immediate solution

for the current lack of energy density in today's batteries and an effective means of propulsion for micro air vehicles are also mentioned. In [21], the flapping wing vehicle is consider as a total system in terms of systems integration and production. The production of the wings by a sterolithography process is proposed and the beating of the wings is proposed to be powered by a reciprocating chemical muscle that directly converts chemical energy to mechanical energy without combustion.

A comprehensive analysis of the bound leading edge vortex on a flapping wing was presented in [9]. This analysis was performed with a CFD Navier-Stokes solver and used periodic flapping kinematics that were functions of sines and cosines. In [9], it was found that the bound vorticity resides primarily at the leading edge of the wing. An extensive study [8] investigated scaling issues for MAVs, lift and thrust characteristics for flapping wings, drag and required power for flapping wing flight and flexible airfoil behavior at low Reynolds numbers. Sinusoidal wing kinematics are discussed in [6], [8] and [10] that describe the orientation of a wing and the angle of attack when considering a constant free stream velocity. In [6], the wing geometries of many avian examples such as seagulls and owls where accurately described using the camber, thickness and chord variation along the wing span. In [10], the 3D unsteady aerodynamics of a pair of flapping wings in a constant free stream are studied. The wings are modeled as rigid and the orientation kinematics of the wings are three angles that vary sinusoidally. The aerodynamic model is a vortex panel model that accounts for bound vorticity as well as the wake effects out to one flapping cycle of the wings. The use of vortex panel methods as an effective means of representing the aerodynamics in flapping wing systems has become fairly common.

In [4], the optimal distribution of vorticity on a flapping wing is solved for with respect to minimizing the power requirements of the wing stroke. A vortex lattice method is used to position bound vortices along the span of the wing and account for the wake up to one wing beat period aft of the vehicle. Three forms of power are included in the calculation of total power, thrust power, induced power and profile power. The thrust power and induced power are functions of the kinetic energy deposited into the wake and the parasitic power is accounted for with a drag coefficient. Comparisons of flapping frequency, flapping amplitude and non-dimensional average power for various average lift and thrust coefficients are included as well as a comparison to actual data taken from birds in flight, [22]. The kinematics of the rigid wings in [4] are assumed to be a sinusoidal flapping motion.

An experimental setup for testing and validating the loads on insect-like flapping wings has been used, [16]. In [16], an unsteady, aeroelastic analysis of insect flight was performed. This formulation consists of a structural dynamics model with a prescribed motion at the root of the wing and an unsteady aerodynamics model including non-circulatory forces. The structural model is a two dimensional flexible plate structure, the dynamic equations of which are solved using an assumed modes method.

In [2], a double appendage, planar system, with two links for each appendage similar to the legs of a frog was modeled. The vehicle was symmetric and was constrained to have symmetric flapping motion. The equations of motion of the vehicle were derived using a Lagrangian approach. The derivation of the equations of motion cleverly included the fluid dynamics in a manner identical to the rigid

body dynamics. The Lagrangian of motion for the fluid was represented in terms of an added inertia on the appendages due to the fluid. The primary purpose of [2] is similar to the work of this thesis and is to illustrate a method for designing an optimal flapping stroke for a vehicle using flapping appendages for locomotion. In [2], the flapping stroke is constrained to be periodic in shape or state space which allows for a repeatable stroke. An optimization framework is used to design the flapping stroke. The cost function is the total control effort used over the flapping cycle divided by the distance traveled by the vehicle. In other words, the goal is to minimize the effort to distance ratio. This problem has path equality and inequality constraints imposed. The path equality constraints are the equations of motion of the vehicle and the fluid. The inequality constraints are the boundaries of the admissible shape space, these boundaries represent limits on the allowable configuration of the vehicle.

The non-sinusoidal path optimization of a flapping airfoil has been studied [3]. In [3], the planar case of an airfoil flapping in an elliptical manner was studied in an optimization framework. This model did not include rigid or flexible body dynamics in the problem formulation. However the aerodynamics were included through a Navier-Stokes solver, this method accurately modeled viscous effects, flow separation effects and unsteady effects. The motion of the airfoil takes place in a constant free stream. The optimization problem here is to maximize total thrust force over the flapping cycle. The thrust force is defined to be opposite the direction of the free stream velocity of the fluid. The optimization parameters describe the two dimensional shape of the wing path over the stroke. The solution is constrained

to behave periodically, thus the flapping stroke must be repeatable.

Considering that flapping wing vehicles represent a very complex problem in sensor technology, multi-body and fluid dynamics, optimization and control, some have elected to study the compilation of these systems as they effect the operation of the entire vehicle [20, 17, 19]. In [19], the aerodynamics are modeled using 3D potential flow theory. The dynamics are modeled in a general way through the use of the Gibbs-Appel equations. The optimization problem of how to move the wings is not discussed in [19], the wing stroke followed is that of the Hawkmoth, *Manduca Sexta*. In [17], an optical sensor model similar to the ocelli of an insect eye is assumed. Control of the vehicle is assumed to be through the wings as well as haltres on the sides of the vehicle. These haltres are an oscillating rotational control mechanism that is utilized by various flying insects. The control system uses a linearized output feedback methodology for inertial position and vehicle orientation tracking. The work of [20] studies an integrative model of insect flight control. Here, detailed rigid body dynamics are used. The inertias of the vehicle are very accurately computed using a 3D solid computer model. The aerodynamic forces and moments are simplified using a linear representation with non-dimensional coefficients. A visual object recognition sensory system is assumed. Haltres are assumed as the orientation control mechanism for the vehicle and tracking control is through the use of a proportional controller.

The preliminary development of a micromechanical flying insect or MFI is discussed in [18]. Here, a higher level perspective is taken. A first approximation to the rigid body dynamics is used that neglects nonlinearities and coupling between the degrees of freedom. The control architecture is considered to be multi-level in

that there are levels from 'mission planner' to 'trajectory planner' to 'flight mode controller', the last and bottom level is the 'wing kinematics controller'. Mission planner level tasks would be tasks such as 'find a trapped victim' for the case of search and rescue. Trajectory planner level tasks are tasks such as optimization of a route to move from the vehicle's current location to where the trapped victim would be. The flight mode controller would be responsible for determining how the kinematics of the vehicle should evolve in order to track the trajectory. The wing kinematics controller is the system that would design and track the motions of the wings so as best to track the vehicle kinematics from the flight mode controller. The method used in this thesis is at the level of the 'flight mode controller' and the 'wing kinematics controller'. The kinematics of the wings in [18] are linear combinations of sinusoids. The control strategy is a bang-bang technique that uses the sign of the total error times the saturated control value.

This thesis is organized as such. First the model of the system is presented, then the various reference frames and the kinematic description of the system are discussed. The equations of motion are then developed using Newton/Euler methods [23]. Next, the aerodynamic model used to calculate the aerodynamic loads on the system is presented. In order to achieve a flight path angle near the desired value, the flapping wing vehicle must move its wings in such a way as to effectively manipulate the aerodynamic forces on its wings without violating path and end constraints. The quality and effectiveness of this motion is measured with a cost function. This cost function and the constraints associated with the problem are discussed. Following this, the example chosen to test the method is discussed. The controller used to

track the state histories from the optimization routine is the derived and its stability is analyzed. Finally, the wing stroke generation, trajectory tracking, linearization and stability results are presented and discussed.

CHAPTER II

THE MODEL

This is a model of a vehicle with motion in the longitudinal plane only. No lateral motion of the vehicle is considered, this means that the vehicle center of mass must remain on a vertical plane and that the velocity vector of the vehicle must also lie on the same plane, App. A. Often traditional stability and control analyses consider the longitudinal and lateral-directional motions of aircraft separately. This is done, not only to simplify the analyses, but also to obtain useful characteristics of traditional flight modes associated with the longitudinal and lateral-directional flight. Longitudinal flight is primarily concerned with the modes of the vehicle that occur as a result of changes in the forward velocity, the angle of attack of the vehicle and the pitch attitude of the vehicle, where as lateral-directional modes occur as a result of the rolling, yawing and sideslip of the vehicle.

The translational motion of the system is described by the velocity vector of the fuselage of the vehicle expressed along inertially fixed axes. The translational dynamics of the fuselage center of mass were chosen because this is the point where the wings are attached and while these dynamics are slightly more complicated than the translational dynamics of the center of mass of the vehicle, the rotational dynamic equations are greatly simplified when expressed in terms of the translation of the fuselage center of mass. Because the vehicle fuselage is modeled as a point mass, it contributes neither rotational inertia about its own mass center or aerodynamic effects.

The wings are modeled as rigid plates that rotate about a shoulder joint with three rotational degrees of freedom, plunge, pitch and sweep. Because the vehicle model is restricted to move longitudinally, the wings must move such that the vehicle velocity remains parallel to the longitudinal plane. The motion of the wings is symmetric with respect to the longitudinal plane. The concept for the type of symmetry used in this model was intuitive, however, the mathematical basis is presented in Chapter III. Conceptually, this symmetry relationship is such that both wings sweep forward together, both wings plunge vertically together and both wing pitch in the same direction. Because the vehicle velocity has no vector component that is perpendicular to the longitudinal plane, this state can be neglected provided that the symmetry relationship used does in fact enforce this result. Another result of enforcing that the system evolve symmetrically is that only the equations of motion of one wing need be considered. If the motions of one wing are known, then by the symmetry relationship, the motions of the other wing are also known. This results in two equations of motion for the motion of the vehicle fuselage and three equations of motion describing the evolution of the wing angular velocities. Three additional equations are required to describe the evolution of the wing Euler Angle orientation. The states of the system are the inertial velocity of the fuselage, the angular velocity of the right wing and the orientation of the right wing,

$$\mathbf{x} = \begin{bmatrix} \mathbf{V}_p \\ \omega_1 \\ \theta_1 \end{bmatrix}. \tag{2.1}$$

The aerodynamics of the wings are assumed to be independent of each other. The aerodynamic model is quasi-steady and $2D$ [14, 15]. This means that the lift and drag forces include contributions from the instantaneous total velocity and the rotation rate of the wing. The non-dimensional lift is computed from a combination of a zero angle of attack term and a total angle of attack dependent term. The lift curve slope is adjusted using a correction for finite span wings, [24]. The non-dimensional drag on the wings is computed using a standard drag polar. This contains a parasitic or profile drag contribution and an induced drag contribution that is a quadratic function of the non-dimensional lift.

The derivative convention is as such, an over dot signifies the derivative of a quantity in its own frame, not the inertial derivative of the quantity. A ${}^{\#}d/dt$ signifies the derivative of a quantity in the # frame. Brackets around a quantity, $[a]_{\#}$ signify that the quantity is expressed in the # frame.

CHAPTER III

REFERENCE FRAMES

Three reference frames are used here. An inertially fixed frame and two wing-fixed frames. When the wings are at the zero orientation, $\theta_1 = \theta_2 = \theta_3 = 0$ all reference frames are parallel. These rotations are detailed in Figs. 1(a)-1(c). The inertial and wing-fixed bases are referred to as, i, 1 and 2 respectively. While one can consider a stability reference frame that describes planar motion in terms of a velocity magnitude and a direction angle, in this case, a velocity and flight path angle, the formulation used here considers only three reference frames. This will be demonstrated as it was part of a previous formulation and offers a slightly different perspective on longitudinal flight. Results will also be presented in this manner, using the velocity and flight path information as it allows for easier and more intuitive analysis. Also in this chapter, the direction cosine matrices and kinematic influence matrices that are used are discussed.

A. Direction cosine matrices

The wing orientations are described using a 3-2-1 Euler angle sequence which is explained in detail in [25]. The cosine matrices, C_{1i} and C_{2i} transform vectors expressed in the inertial frame to vectors expressed in the 1 and 2 frames respectively [25]. These matrices are

$$C_{1,2} = \begin{bmatrix} c\theta_2 c\theta_3 & c\theta_2 s\theta_3 & -s\theta_2 \\ s\theta_1 s\theta_2 c\theta_3 - c\theta_1 s\theta_3 & s\theta_1 s\theta_2 s\theta_3 + c\theta_1 c\theta_3 & s\theta_1 c\theta_2 \\ c\theta_1 s\theta_2 c\theta_3 + s\theta_1 s\theta_3 & c\theta_1 s\theta_2 s\theta_3 - s\theta_1 c\theta_3 & c\theta_1 c\theta_2 \end{bmatrix} \tag{3.1}$$

In Eq. 3.1, the notation $c = \cos$, $s = \sin$, is used and θ_i refers to the Euler angles of the 1 or 2 wing. Each wing has associated with it, a direction cosine matrix that changes with the orientation of the wing and thus with time. The next section will describe the motion and kinematics of the various reference frames.

B. Reference frame kinematics

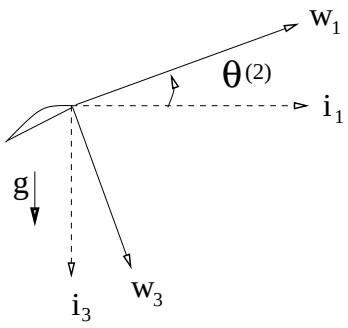

(a) Rotation about 2-axis

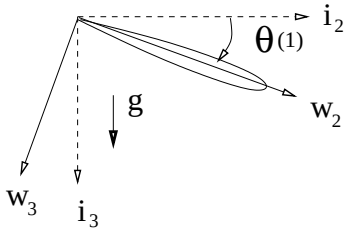

(b) Rotation about 1-axis

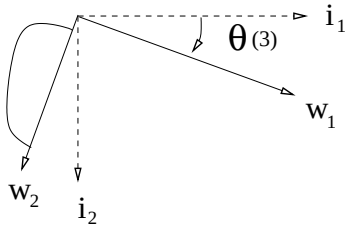

(c) Rotation about 3-axis

Fig. 1. Reference frame visualization for wing 1.

This section describes the kinematics of the rotation of the various reference frames. When all rotation angles are zero, the 1-frame, 2-frame and inertial frame have parallel 1, 2 and 3 bases. The orientation of the 1-frame and 2-frame relative to the inertial frame are described by two 3-2-1 Euler angle sets, θ_1 and θ_2 respectively. Where $\theta_i(1)$, $\theta_i(2)$ and $\theta_i(3)$ are the rotations about the intermediate 1, 2 and 3 axes. Angular velocities are about wing-fixed axes. The wing orientations must be symmetrical with respect to the inertial 1-3 plane. The symmetry relationship imposed is as follows,

$$\theta_2 = [-\theta_1(1), \theta_1(2), -\theta_1(3)]^T \tag{3.2}$$

$$= [T]\theta_1 \tag{3.3}$$

where

$$[T] = \begin{bmatrix} -1 & 0 & 0 \\ 0 & 1 & 0 \\ 0 & 0 & -1 \end{bmatrix}$$

Qualitatively, the symmetry relationship in Eq. 3.3 says that the wings plunge up and down together, the wings pitch in the same direction and the wings sweep forward and backward together. This is intuitive if these rotations are considered separately. The symmetric plunging of the wings is commonly known as wing dihedral for fixed wing aircraft. The symmetric pitch is known as the angle of attack of the wings relative to the fuselage of the vehicle. Here, all rotations are relative to

the inertial frame. The symmetric sweep of the wings is commonly known as wing sweep. This symmetry relationship is standard for most fixed wing aircraft. Because $[T]$ is constant,

$$\dot{\theta}_2 = [T]\dot{\theta}_1. \tag{3.4}$$

From [25], the kinematics for wing 1 and 2 are

$$\omega_1 = [B_1(\theta_1)]\dot{\theta}_1 \tag{3.5}$$

$$\dot{\theta}_1 = [A_1(\theta_1)]\omega_1 \tag{3.6}$$

$$\omega_2 = [B_2(\theta_2)]\dot{\theta}_2 \tag{3.7}$$

$$\dot{\theta}_2 = [A_2(\theta_2)]\omega_2 \tag{3.8}$$

The kinematic influence matrix A, is a function of only the second and third rotations. The matrix A is a time varying transformation that maps the angular velocities of a rotating rigid body (i.e. a wing) expressed in a frame fixed to that body into the time rate of change of the parameters used to describe the orientation of that body relative to another reference frame (i.e. the inertial frame). This mapping is a function of only the rotations about the intermediate 2 and 1 axes and becomes singular if the second orientation parameter, $\theta(2)$, goes to 90°. Chapter VI explains how this is dealt with in more detail. The expression for the kinematic influence matrix A is

$$A_{1,2} = \frac{1}{c\theta(2)} \begin{bmatrix} c\theta(2) & s\theta(2)s\theta(1) & s\theta(2)c\theta(1) \\ 0 & c\theta(2)c\theta(1) & -c\theta(2)s\theta(1) \\ 0 & s\theta(1) & c\theta(1) \end{bmatrix} \tag{3.9}$$

We seek an expression for ω_2 in terms of ω_1. The symmetry relationship used to map the angular velocities of the 1-frame into the angular velocities of the 2-frame *must not* violate Eqs. 3.3, 3.6 and 3.8. First, assume that the angular velocity symmetry relation,

$$\omega_2 = [T]\omega_1 \tag{3.10}$$

does not violate Eqs. 3.3, 3.6 and 3.8. This relationship states that the angular velocity of wing 2 projected on the 1 and 3 axes of the 2-frame are opposite that of wing 1 projected on the 1 and 3 axes of the 1-frame. It also says that the angular velocity of wing 1 projected onto the 2 axis of the 1-frame is equal to the angular velocity of wing 2 projected onto the 2 axis of the 2-frame.We will now proceed to show that this is indeed true and that the symmetry relation in Eq. 3.10 is the mapping between the angular velocities of the 1-frame and the 2-frame.

We begin by substituting the kinematics in Eq. 3.6 into the symmetry relation in Eq. 3.4 to obtain,

$$A(\theta_2)\omega_2 = [T]A(\theta_1)\omega_1 \tag{3.11}$$

For the symmetry relation in Eq. 3.10 to hold, the following must be true,

$$A(\theta_2)[T]\omega_1 = [T]A(\theta_1)\omega_1. \tag{3.12}$$

From this, it follows that

$$A([T]\theta_1)[T] = [T]A(\theta_1) \tag{3.13}$$

must also hold. If Eq. 3.13 is true, then it follows that Eq. 3.10 is the symmetry relationship between the angular velocities of the first and second wing that abide by Euler Angle symmetry specified in Eq. 3.3. Evaluating the left and right hand sides of Eq. 3.13, we obtain,

$$A([T]\theta_1)[T] = \frac{1}{c\theta_1(2)} \begin{bmatrix} -c\theta_1(2) & -s\theta_1(2)s\theta_1(1) & -s\theta_1(2)c\theta_1(1) \\ 0 & c\theta_1(2)c\theta_1(1) & -c\theta_1(2)s\theta_1(1) \\ 0 & -s\theta_1(1) & -c\theta_1(1) \end{bmatrix} \tag{3.14}$$

and

$$[T]A(\theta_1) = \frac{1}{c\theta_1(2)} \begin{bmatrix} -c\theta_1(2) & -s\theta_1(2)s\theta_1(1) & -s\theta_1(2)c\theta_1(1) \\ 0 & c\theta_1(2)c\theta_1(1) & -c\theta_1(2)s\theta_1(1) \\ 0 & -s\theta_1(1) & -c\theta_1(1) \end{bmatrix} \tag{3.15}$$

and these two terms are indeed equal, thus the relation in Eq. 3.13 holds and Eq. 3.10 is the symmetry relation describing the angular velocity kinematics of one wing

in terms of the other. Again, because the transformation $[T]$ is time invariant, the relationship between the angular velocity rates is identical to that of the Euler Angle rates and is as follows,

$$\dot{\omega}_2 = [T]\dot{\omega}_1. \tag{3.16}$$

CHAPTER IV

VEHICLE DYNAMICS

A. Translational equations of motion

Here, the longitudinal translational equations of motion for the system are developed. First the development of the translational equations of motion will proceed using the flight path velocity and flight path angle states to describe the translation of the center of mass. The second development will describe the translation of the vehicle fuselage, which is represented as a point mass, using inertial velocity states. The second development is more general and is the one chosen to describe the translational dynamics of the system. The rigid body equations of motion will be developed using Newton-Euler momentum methods similar to [23].

1. Translation of mass center

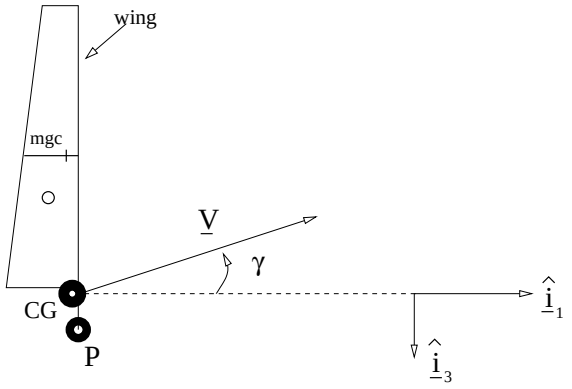

Fig. 2. System translation relative to inertial frame.

Fig. 2 illustrates the translation of the center of mass of the system. The

stability frame offers a convenient frame to express the equations in as the 1-axis of this frame is aligned with the velocity vector of the system center of mass by definition. The resulting translational equations also end up to be quite convenient. The translational momentum of the system in terms of the center of mass of the system can be written as

$$[\mathbf{p}]_s = mV\hat{\mathbf{s}}_1 \tag{4.1}$$

This is the total inertial momentum of the system as seen in the stability frame. The inertial derivative of Eq. 4.1 is

$$[\frac{{}^i d}{dt}\mathbf{p}]_s = m\frac{{}^s d}{dt}([\mathbf{V}]_s) + m\dot{\gamma}\hat{\mathbf{s}}_2 \times V\hat{\mathbf{s}}_1 \tag{4.2}$$

Eq. 4.2 can be rewritten as

$$[\frac{{}^i d}{dt}\mathbf{p}]_s = m\dot{V}\hat{\mathbf{s}}_1 - m\dot{\gamma}V\hat{\mathbf{s}}_3 \tag{4.3}$$

where γ is the vehicle flight path angle. This development is only valid for vehicle motion in the longitudinal plane as a result of the cross product of the rotation of the stability frame relative to the inertial frame with the vehicle velocity vector. In general, the rotation of the stability frame relative to the inertial frame is a function of the flight path angle rate and the heading angle rate. For this case the heading angle rate is zero because the vehicle is restricted to longitudinal motion. By Newton's

second law

$$[\overset{i}{\frac{d}{dt}}\mathbf{p}]_s = [\sum \mathbf{F}]_s \tag{4.4}$$

Because only longitudinal motion is permitted, there must be no forces in the stability-2 direction. Using this and Eqs. 4.3 and 4.4, we have

$$\dot{V} = \frac{1}{m}\sum \mathbf{F}\hat{\mathbf{s}}_1 \tag{4.5}$$

$$\dot{\gamma} = -\frac{1}{mV}\sum \mathbf{F}\hat{\mathbf{s}}_3 \tag{4.6}$$

Eqs. 4.5 and 4.6 describe the translation of the vehicle CG in the longitudinal plane. The forces in the stability 1 and 3 directions are sums of the aerodynamic forces on the vehicle, from both wings, and the gravitational force. The next development describes the translation of the fuselage and is not restricted to motion in the longitudinal plane.

2. Translation of fuselage

Fig. 3 illustrates the translation of the fuselage of the vehicle relative to the inertial frame. Recall that the mass center of the vehicle, in general, does not coincide with the fuselage. The development again begins with translational momentum. The translational momentum of the fuselage expressed in the inertial frame is

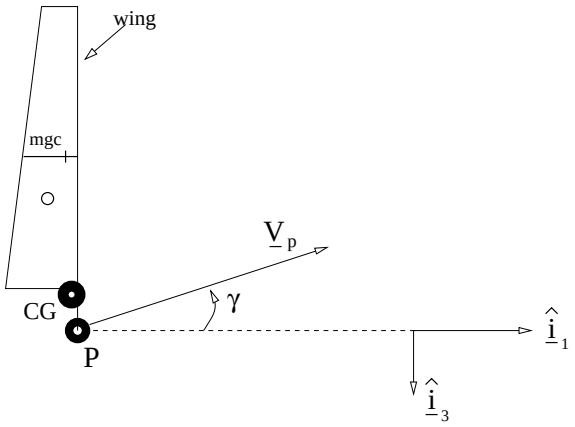

Fig. 3. Fuselage translation relative to inertial frame.

$$[\mathbf{p}_p]_i = m_p[\mathbf{V}_p]_i \tag{4.7}$$

Upon taking the inertial derivative of Eq. 4.7 and applying Newton's second law, the following is obtained

$$\begin{aligned} \frac{^i d}{dt}(\mathbf{P}_p) &= \sum \mathbf{F}_p \\ &= \mathbf{R}_1 + \mathbf{R}_2 + m_p\mathbf{g} \end{aligned} \tag{4.8}$$

Notice that this formulation is much more general in that it considers a general vehicle velocity that could have a component perpendicular to the longitudinal plane. Also notice the lack of a cross product, this is because the velocity vector is expressed in a frame that is not rotating relative to the inertial frame. The symmetry of rotational motion for the system will be imposed later. The vectors $\mathbf{R}_1$ and $\mathbf{R}_2$ are the reaction forces exerted on the point mass by wings 1 and 2 respectively.

These reactions plus the force of gravity are the only forces acting on the vehicle fuselage. However, we desire that the translational equations of motion be in terms of the states of the system, the velocity of the fuselage, the angular velocity and angular orientation of the wings. To achieve this, the reactions must be determined as functions of the motions of the wings and substituted into Eq. 4.8. We begin with the translational momentum of wing 1.

$$\mathbf{P}_1 = m_1 \mathbf{v}_1 \tag{4.9}$$

The inertial velocity of the wing, $\mathbf{v}_1$, is a function of the velocity of the fuselage and a velocity due to the rotation of the wing about point P.

$$\begin{aligned} \mathbf{v}_1 &= \mathbf{V}_p + \frac{^i d}{dt}(\mathbf{d}_{c_1}) && (4.10) \\ \frac{^i d}{dt}(\mathbf{d}_{c_1}) &= \omega_1 \times \mathbf{d}_{c_1} && (4.11) \end{aligned}$$

The development proceeds as previously by taking the inertial derivative of the translational momentum of the wing and evoking Newton's second law. The inertial derivative of the translational momentum of the wing is

$$\begin{aligned} \frac{^i d}{dt}(\mathbf{P}_1) &= m_1 \left(\frac{^i d}{dt}(\mathbf{V}_p) + \frac{^i d}{dt}(\omega_1 \times \mathbf{d}_{c_1}) \right) && (4.12) \\ \frac{^i d}{dt}(\omega_1 \times \mathbf{d}_{c_1}) &= \frac{^i d}{dt}(\omega_1) \times \mathbf{d}_{c_1} + \omega_1 \times \frac{^i d}{dt}(\mathbf{d}_{c_1}) && (4.13) \end{aligned}$$

To obtain a more convenient expression for the inertial momentum rate, we

reorder the cross product in the $\frac{^id}{dt}(\omega_1)$ term and make use of the cross product tensor representation $[\omega^\times]$, where pre-multiplication of a vector by $[\omega^\times]$ performs the cross product operation of ω with the vector. The inertialal translation momentum rate of the wing becomes

$$\frac{^id}{dt}(\mathbf{P}_1) = m_1 \left(\frac{^id}{dt}(\mathbf{V}_p) - [\mathbf{d}_{c_1}^\times]\dot{\omega}_1 + [\omega_1^\times][\omega_1^\times]\mathbf{d}_{c_1} \right), \tag{4.14}$$

where,

$$[\omega^\times] = \begin{bmatrix} 0 & -\omega_3 & \omega_2 \\ \omega_3 & 0 & -\omega_1 \\ -\omega_2 & \omega_1 & 0 \end{bmatrix}. \tag{4.15}$$

By Newton's second law, we set the inertial time rate of change of the wing translational momentum equal to the sum of the forces acting on the wing. This includes, the reaction associated with that wing, but in the opposite direction of that acting on the fuselage, the sum of all aerodynamic forces acting on the wing, and the force of gravity. The following equation results

$$\begin{aligned} \frac{^id}{dt}(\mathbf{P}_1) &= \sum \mathbf{F}_1, & (4.16) \\ &= -\mathbf{R}_1 + \mathbf{F}_{A_1} + m_1\mathbf{g}. & (4.17) \end{aligned}$$

The reactions are solved for to obtain

$$\mathbf{R}_1 = -\frac{^id}{dt}(\mathbf{P}_1) + \mathbf{F}_{A_1} + m_1\mathbf{g}. \tag{4.18}$$

An expression for the equations of motion in Eq. 4.8 in terms of the motion of the two wings is sought. To obtain this, it is first realized that the translational momentum rate equation for the second wing is identical to that of the first wing save replacing the 1 subscripts with 2 subscripts. Eqs. 4.14 and 4.18 are substituted into Eq. 4.8 to get

$$\begin{aligned} m_p \frac{^i d}{dt}(\mathbf{V}_p) = &- m_1 \left(\frac{^i d}{dt}(\mathbf{V}_p) - [\mathbf{d}_{c_1}^{\times}]\dot{\omega}_1 + [\omega_1^{\times}][\omega_1^{\times}]\mathbf{d}_{c_1} \right) \\ &- m_2 \left(\frac{^i d}{dt}(\mathbf{V}_p) - [\mathbf{d}_{c_2}^{\times}]\dot{\omega}_2 + [\omega_2^{\times}][\omega_2^{\times}]\mathbf{d}_{c_2} \right) \\ &+ \mathbf{F}_{A_1} + \mathbf{F}_{A_2} + m_1\mathbf{g} + m_2\mathbf{g} + m_p\mathbf{g} \end{aligned} \tag{4.19}$$

Upon rearranging, what was desired is achieved.

$$\begin{aligned} m\frac{^i d}{dt}(\mathbf{V}_p) - m_1[\mathbf{d}_{c_1}^{\times}]\dot{\omega}_1 - m_2[\mathbf{d}_{c_2}^{\times}]\dot{\omega}_2 \\ + m_1[\omega_1^{\times}][\omega_1^{\times}]\mathbf{d}_{c_1} + m_2[\omega_2^{\times}][\omega_2^{\times}]\mathbf{d}_{c_2} = \sum \mathbf{F}_A + m\mathbf{g} \end{aligned} \tag{4.20}$$

or

$$\begin{aligned} m\frac{^i d}{dt}(\mathbf{V}_p) - (m_1[\mathbf{d}_{c_1}^{\times}]\dot{\omega}_1 + m_2[\mathbf{d}_{c_2}^{\times}]\dot{\omega}_2) \\ + (m_1[\omega_1^{\times}]^2\mathbf{d}_{c_1} + m_2[\omega_2^{\times}]^2\mathbf{d}_{c_2}) = \sum \mathbf{F}_A + m\mathbf{g} \end{aligned} \tag{4.21}$$

Eq. 4.21 is the equation of motion for the fuselage. It contains the mass, translational acceleration product as well as other terms that are readily recognizable. The $\dot{\omega}$ terms are the tangential acceleration terms due to the rotational acceleration of the wings. The $[\omega^{\times}]^2$ terms are the centripetal acceleration terms due to the

angular velocity of the wings. And the total aerodynamic force on the vehicle and the total gravitational force on the vehicle are on the right hand side. Notice that unlike Eqs. 4.5 and 4.6, here it was not assumed that the system moves only in the longitudinal plane where Eqs. 4.5 and 4.6 were developed assuming that the angular velocity of the stability frame relative to the inertial frame is $\dot{\gamma}$.

For the sake of completeness, the next development will detail the collapse of Eq. 4.21 into the standard $\mathbf{F} = m\mathbf{a}$ that is obtained when the translational equations of motion are written with respect to the center of mass of the system. To begin with, the acceleration of the fuselage is represented in terms of the acceleration of the center of mass of the vehicle. The inertial position vector for the fuselage is

$$\mathbf{r}_p = \mathbf{r}_c + \mathbf{r}_{pc} \tag{4.22}$$

where $\mathbf{r}_{pc}$ is the position of the fuselage relative to the system center of mass. From this, Eq. 4.22 is differentiated to obtain the expression for the inertial acceleration of the point mass in terms of the acceleration of the system mass center and the acceleration of the fuselage relative to the system mass center. Thus, we have

$$\frac{^i d^2}{dt^2}(\mathbf{r}_p) = \frac{^i d^2}{dt^2}(\mathbf{r}_c) + \frac{^i d^2}{dt^2}(\mathbf{r}_{pc}) \tag{4.23}$$

At this point, it is desired to have an expression for the acceleration of the fuselage relative to the center of mass of the system, $\ddot{\mathbf{r}}_{pc}$. This is an inertial derivative. By the definition of center of mass,

$$m_p\mathbf{r}_{pc} + m_1(\mathbf{r}_{pc} + \mathbf{d}_{c_1}) + m_2(\mathbf{r}_{pc} + \mathbf{d}_{c_2}) = 0. \tag{4.24}$$

Eq. 4.24 leads to,

$$(m_p + m_1 + m_2)\mathbf{r}_{pc} + m_1\mathbf{d}_{c_1} + m_2\mathbf{d}_{c_2} = 0, \tag{4.25}$$

from which comes,

$$\mathbf{r}_{pc} = -\frac{1}{m}(m_1\mathbf{d}_{c_1} + m_2\mathbf{d}_{c_2}). \tag{4.26}$$

The first derivative of $\mathbf{r}_{pc}$ is

$$\dot{\mathbf{r}}_{pc} = -\frac{1}{m}(m_1\omega_1 \times \mathbf{d}_{c_1} + m_2\omega_2 \times \mathbf{d}_{c_2}) \tag{4.27}$$

the second derivative of $\mathbf{r}_{pc}$ is

$$\begin{aligned}\ddot{\mathbf{r}}_{pc} =& \frac{1}{m}(m_1[\mathbf{d}_{c_1}^{\times}]\dot{\omega}_1 + m_2[\mathbf{d}_{c_2}^{\times}]\dot{\omega}_2) \\ &- \frac{1}{m}(m_1[\omega_1^{\times}]^2\mathbf{d}_{c_1} + m_2[\omega_2^{\times}]^2\mathbf{d}_{c_2}),\end{aligned} \tag{4.28}$$

where the $\dot{\omega}$ cross products have be switched and the cross product tensor representation has been used. Notice the striking similarities between Eqs. 4.21 and 4.28. Upon substituting Eq. 4.23 and 4.28 into the equation of motion in Eq. 4.21 we recover the translational equation of motion for the center of mass of the system.

$$m\frac{^i d}{dt}(\mathbf{V}_c) = \sum \mathbf{F}_A + m\mathbf{g} \tag{4.29}$$

B. Wing rotation equations

Each wing has a plunge, pitch and sweep degree of freedom. These are the rotations about the wing-fixed 1, 2 and 3 axes respectively. Fig. 4 shows a tail view of the aircraft and demonstrates the plunge wing deflection as well as the rotation convention of the two wing fixed frames. Three rotational equations of motion and three kinematic equations are needed to describe the evolution of a wing's angular velocities and orientation relative to the inertial frame.

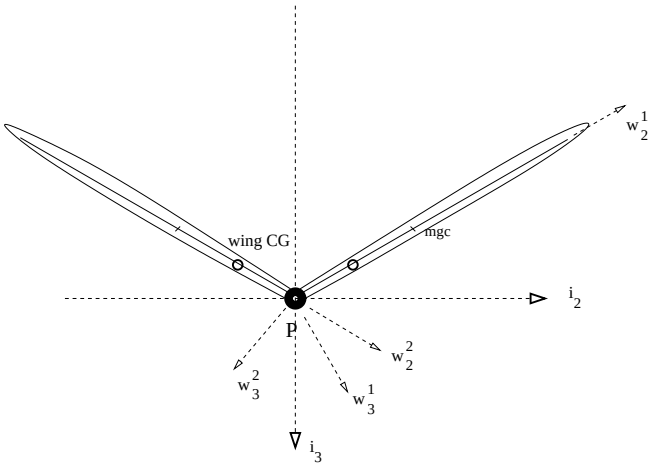

Fig. 4. Wing frames.

From [26], the relative angular momentum of the wing about the arbitrary point, P, is

$$\mathbf{H}_1 = \mathbf{I}_{c_1}\omega_1 + \mathbf{d}_{c_1} \times (m_1 \frac{^i d}{dt}(\mathbf{d}_{c_1})) \tag{4.30}$$

The first term on the right hand side of Eq. 4.30 represents the rotational momentum of the wing about its center of mass and the second term represents the moment of

the relative translational momentum of the wing about point P. The inertial velocity of the wing relative to point P can be seen in Eq. 4.11.

Also from [26], there is the inertial derivative of angular momentum for a rigid body rotating about an arbitrary, inertially accelerating point. In general, this expression contains more than the external moments acting on the body.

$$\frac{^i d}{dt}(\mathbf{H}_1)|_p = \sum \mathbf{L}|_p + m_1 \frac{^i d}{dt}(\mathbf{V}_p) \times \mathbf{d}_{c_1} \tag{4.31}$$

The inertial time derivative of the body's angular momentum is

$$\frac{^i d}{dt}(\mathbf{H}_1) = \frac{^1 d}{dt}(\mathbf{H}_1) + \omega_1 \times \mathbf{H}_1 \tag{4.32}$$

Performing the differentiation of Eq. 4.30 yields,

$$\begin{aligned} \frac{^i d}{dt}(\mathbf{H}_1) = {} & I_1 \dot{\omega}_1 + m_1 \mathbf{d}_{c_1} \times \dot{\omega}_1 \times \mathbf{d}_{c_1} \\ & + \omega_1 \times I_1 \omega_1 + m_1 \omega_1 \times \mathbf{d}_{c_1} \times \omega_1 \times \mathbf{d}_{c_1} \end{aligned} \tag{4.33}$$

Note that the over dots in Eq. 4.33 indicate a derivative in the 1-frame. Upon rearranging the cross products in the second and fourth terms on the right hand side of Eq. 4.33 and substituting the result into Eq. 4.31, the following is obtained,

$$(I_1 - m_1[\mathbf{d}_{c_1}^{\times}]^2)\dot{\omega} + [\omega_1^{\times}](I_1 - m_1[\mathbf{d}_{c_1}^{\times}]^2)\omega + m_1[\mathbf{d}_{c_1}^{\times}]\frac{^i d}{dt}(\mathbf{V}_p) = \mathbf{u}_1 + \mathbf{M}_{A_1} \tag{4.34}$$

This is the equation of motion for one wing. The development for the other wing is identical. The three control moments on the wing along the wing-fixed axes

are $\mathbf{u}_1$. The three control moments act at point P. The moments $\mathbf{M}_{A_1}$ are the sum of the aerodynamic moments on the wing in wing 1 axes. Notice the similarity of Eq. 4.34 to Euler's equations for the rotation of a rigid body. If the point P does not accelerate inertially, these equations are reduced to the rotation of a rigid body about a point other than its mass center. This result is similar to the parallel axis theorem for planar rotations. Eqs. 4.21 and 4.34 are the acceleration level equations governing the evolution of the flapping wing system. To be useful however, each set of equations must be expressed in a single frame. Eq. 4.21 are expressed in inertial axes and Eq. 4.34 are expressed in 1-frame axes.

C. State space representation of governing equations

Here we present the equations of motion as well as the kinematic equations in state space form. This is the form that is used as the path equality constraints for the trajectory optimization. Note that the control input appears affinely in Eq. 4.34. We write the state space form of the equations of motion as

$$\dot{\mathbf{x}} = \mathbf{F}(\mathbf{x}) + [G(\mathbf{x})]\mathbf{u}, \tag{4.35}$$

$$\mathbf{F} = [M]^{-1} \begin{pmatrix} \sum \mathbf{F}_A + m\mathbf{g} - m_1[\omega_1^\times]^2\mathbf{d}_{c_1} - m_2[([T]\omega_1)^\times]^2\mathbf{d}_{c_2} \\ \mathbf{M}_{A_1} - [\omega_1^\times](I_1 - m_1[\mathbf{d}_{c_1}^\times]^2)\omega_1 \\ A(\theta_1)\omega_1 \end{pmatrix}. \tag{4.36}$$

The non-square control influence matrix is

$$[G] = [M]^{-1} \begin{pmatrix} \mathbf{0} \\ \mathbf{1} \\ \mathbf{0} \end{pmatrix}. \tag{4.37}$$

The invertible acceleration coupling matrix $[M]$, contains the influence of the vehicle fuselage acceleration on the angular momentum rate of wing 1 as well as the influence of the angular momentum rates on the inertial velocity of the fuselage. $[M]$ is,

$$[M] = \begin{bmatrix} m\mathbf{1} & -(m_1[\mathbf{d}_{c_1}^{\times}] + m_2[\mathbf{d}_{c_2}^{\times}][T]) & \mathbf{0} \\ m_1[\mathbf{d}_{c_1}^{\times}] & (I_1 - m_1[\mathbf{d}_{c_1}^{\times}]^2) & \mathbf{0} \\ \mathbf{0} & \mathbf{0} & \mathbf{1} \end{bmatrix}. \tag{4.38}$$

CHAPTER V

VEHICLE AERODYNAMICS

The aerodynamics of the vehicle are functions of the lift and drag forces on the wings. The fuselage is modeled as a point mass and does not contribute to the aerodynamics of the vehicle. All aerodynamic forces acting on a wing are assumed to act at the mean geometric quarter chord, mgqc, of the wing [14]. The aerodynamic forces include lift and drag forces. The lift force is perpendicular to the instantaneous inertial velocity of the wing and the drag force is parallel to the instantaneous velocity of the wing. These forces are computed in the wing-fixed frame.

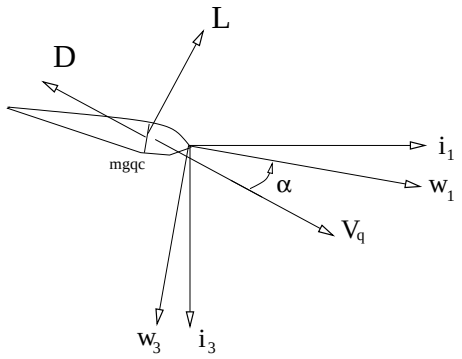

Fig. 5. Aerodynamic forces on a wing.

The forces on a wing are computed using the total inertial velocity of the wing mgqc and as such, include the contributions to the velocity from the angular velocity of the wing. This is a quasi-steady approach. It does not include contributions

from shed vortices, accelerations or added mass, viscous effects, separation or stall, or phase lag effects that occur with higher reduced frequencies. The formulation is modular, a pre-existing aerodynamic model could be used fairly easily. The lift and drag on a wing are defined as

$$L = QSC_L, \tag{5.1}$$

$$D = QSC_D, \tag{5.2}$$

$$Q = \frac{1}{2}\rho \mathbf{v}_q^T \mathbf{v}_q. \tag{5.3}$$

The quantity Q is the instantaneous dynamic pressure at the wing mean geometric quarter chord and the vector $\mathbf{v}_q$ is the inertial velocity of the mgqc and is computed as

$$\mathbf{v}_q = \mathbf{V}_p + \frac{^i d}{dt}(\mathbf{d}_{q_1}), \tag{5.4}$$

$$\frac{^i d}{dt}(\mathbf{d}_{q_1}) = \omega_1 \times \mathbf{d}_{q_1}. \tag{5.5}$$

The non-dimensional lift, C_L, is composed of a zero angle of attack contribution and a dependence on the instantaneous effective angle of attack. The non-dimensional drag is computed using a standard drag polar composed of a zero lift contribution and an induced drag [14]. The non-dimensional lift and drag are defined as

$$C_L = C_{L_0} + C_{L_\alpha}\alpha_{eff}, \tag{5.6}$$

$$C_D = C_{D_0} + RC_L^2, \tag{5.7}$$

where the effective angle of attack, α_{eff} and R are

$$\alpha_{eff} = \arctan\left(\frac{\mathbf{v}_q(3)}{\mathbf{v}_q(1)}\right), \tag{5.8}$$

$$R = \frac{1}{\pi e AR}. \tag{5.9}$$

Note that only flow parallel to the mean geometric chord is considered in the angle of attack computation. Eqs. 5.1 and 5.2 present the scalar magnitudes of the lift and drag vectors. The instantaneous vectors are computed in the wing-fixed frame as

$$[\mathbf{L}] = L[\sin\alpha_{eff}, 0, -\cos\alpha_{eff}]^T, \tag{5.10}$$

$$[\mathbf{D}] = -D\frac{[\mathbf{v}_q]}{\parallel \mathbf{v}_q \parallel}. \tag{5.11}$$

The aerodynamic moments on the wing are considered to be simply a function of the lift and drag terms above. There is no consideration of non-circulatory terms in the aerodynamics. Pure aerodynamic moments about the wing aerodynamic center are also not included, it is assumed that the wing has zero camber and is symmetric about the camber line [15]. The moments on the wing due to the aerodynamics are

$$\mathbf{M}_A = [\mathbf{d}_q^{\times}]([\mathbf{L}] + [\mathbf{D}]). \tag{5.12}$$

CHAPTER VI

WING STROKE OPTIMIZATION

A. Optimal control problem

Here, the optimal control problem or OCP, is posed to design a wing stroke to maintain the flight path and velocity for a flapping wing vehicle of the type discussed in Chapter II. This section presents a cost function and constraints that help to achieve this objective. The optimal control problem can be stated as such

$$\min_{\mathbf{x},\mathbf{u}} J$$

subject to

$$\dot{\mathbf{x}} = \mathbf{f}(\mathbf{x}, \mathbf{u}) \tag{6.1}$$

$$\psi(x_0, x_f, \dot{x}_0, \dot{x}_f) = 0 \tag{6.2}$$

$$\mathbf{g}_{min} \leq \mathbf{g}(\mathbf{x}) \leq \mathbf{g}_{max} \tag{6.3}$$

$$\mathbf{h}_{min} \leq \mathbf{h}(\mathbf{x}) \leq \mathbf{h}_{max} \tag{6.4}$$

Where the function $\psi(x_0, x_f, \dot{x}_0, \dot{x}_f)$ is a function of the initial and final states of the system and their derivatives, and is responsible for causing the solution to behave cyclically. The function $\mathbf{g}(\mathbf{x})$ are the nonlinear inequality, path constraints that will later function to limit the angle of attack. The function $\mathbf{h}(\mathbf{x})$ are the linear path constraints that will later function to limit the Euler angle orientation of the

wings.

1. Performance index

The performance index used is a measure of the fuselage flight path angle deviation from a desired flight path angle over the course of one stroke period, a measure of the deviation of the flight path velocity from the desired, and a measure of the control rate [27], or 'spikiness' of the control input. This Lagrange type cost function is

$$J = \int_{t_0}^{t_0+T} (\gamma(t) - \gamma_r)^2 + \beta_1 (V_{fp}(t) - V_r)^2 + \beta_2 \dot{\mathbf{u}}(t)^T \dot{\mathbf{u}}(t) dt, \tag{6.5}$$

where,

$$\gamma = -\arctan\left(\frac{V(3)}{V(1)}\right), \tag{6.6}$$

and

$$V_{fp} = \sqrt{\mathbf{V}(1)^2 + \mathbf{V}(3)^2}. \tag{6.7}$$

The first term of the integrand penalizes the flight path angle error over the period of the wing stroke. The second term penalizes the flight path velocity error over the period of the wing stroke. The third term penalizes the control rate and is responsible for smoothing out control effort peaks over the wing stroke. The scalar constants β_1 and β_2 are weightings that are used to specify the relative importance of the velocity tracking error and control rate in the cost function. This is a fixed final time problem. The stroke period is pre-specified. The purpose of this flight

path angle dependent performance index is to have the vehicle maintain a condition as close to translational trim as possible. The constraints that assist in finding a solution that meets this criteria are discussed in the following section.

2. Constraints

First, the system is constrained to behave in a periodic manner. This is done to ensure that tracking the wing stroke repeatedly will result in trimming the vehicle. Specifically, this means that the values of the states and their derivatives must be equal at t_i and $t_i + T$. This constraint manifests as an end constraint, more specifically, a smoothness constraint on the states. The imposed smoothness of the solution is of order 1. It is required that

$$\mathbf{x}(t_i) = \mathbf{x}(t_f) \tag{6.8}$$

$$\dot{\mathbf{x}}(t_i) = \dot{\mathbf{x}}(t_f) \tag{6.9}$$

Here, the i and f subscripts denote the values of the quantities at $t = t_i$ and $t = t_i + T$. Eq. 4.35 represent the path equality constraints governing the time evolution of the system. The solution to the optimal control problem must not violate the dynamics of the system.

The above equality constraints are enough to satisfy the equations of motion and the periodic solution constraints. However, an aerodynamic model is used that assumes a linear lift curve slope and does not account for the effects of separation, departure or stall. To insure that the solution does not violate the bounds of the

assumed aerodynamics, a nonlinear, inequality constraint is imposed.

$$\alpha_{min} \leq \alpha_{eff} \leq \alpha_{max} \tag{6.10}$$

The effective angle of attack, α_{eff} is a nonlinear function of the states, Eq. 5.8. The aerodynamics of an oscillating wing can also be heavily influenced by the reduced frequency, k, of the oscillating wing, [15]. This is a non-dimensional frequency of oscillation of the wing and is a function of the wing beat period, the fluid velocity and the wing mean geometric chord. The reduced frequency effects that occur can reduce the loads on the wing and influence the phasing between when the loads occur and the motion that causes the loads [15]. Effects due to the reduced frequency are not included.

One limitation of the Euler angle kinematics is the singularity of the kinematic influence matrix, $[A(\theta)]$, when the second Euler angle, $\theta(2)$ approaches $\pi/2$. No attempt is made to switch the kinematics as the orientation approaches the singularity. Instead, upper and lower bounds on the Euler angles are imposed at every point of the solution.

$$\theta_{min} \leq \theta \leq \theta_{max} \tag{6.11}$$

The orientation singularity is not the only concern associated with the Euler angle kinematics. Limitations not only on the second rotation, pitch, but on all three rotations are essential in order to obtain a physically significant solution. For example, the wings' sweep, $\theta(3)$, and plunge, $\theta(1)$, angles should not result in the wings crossing each other. The magnitude of the wing plunge angles should not

exceed $\pi/2$. In other words, the wings must remain on their respective sides of the longitudinal plane.

B. NLP representation

The optimal control problem presented above is complex and rife with nonlinearity in the kinematics, equations of motion and the angle of attack constraints. The problem has upper and lower bounds on the wing orientations as well as end conditions that link the initial and final solution values. For these reasons, this problem is converted to a nonlinear programming problem or NLP, and solved numerically. The problem is discretized to represent the problem as a set of finite parameter sequences where the values of the trajectory at discrete points in time, along the stroke period, can be determined that represent a near optimal solution.

Two methods have been used to convert this optimal control problem into an NLP. The first was a standard collocation method that involves using a finite difference approximation to the derivative of the state variables to satisfy the equations of motion at the midpoints between the nodes. The second, a Chebyshev pseudospectral method that allows for the exact determination of the derivative of the states and controls at the nodes corresponding to the extrema of the Nth-order Chebyshev polynomial. The last method is the one currently being used for discretization of the OCP.

1. Classical collocation discretization

The classical collocation method was used as a preliminary means of obtaining a solution. This method is the simplest method of discretizing continuous optimal control problems, for this reason, it was chosen as a first cut at a solution. Conceptually, this method uses the midpoint rule for discretization. A finite number of points are chosen along the trajectory of each state and the constraints in the inequalities, 6.10 and 6.11 are satisfied at these nodes. The dynamics are satisfied in between nodes. In this method, the derivatives of the states are approximated using the midpoint rule where the slope of the function at the midpoint between any two nodes is assumed to be equal to the difference of the function values on either side of the midpoint divided by the time step between the nodes. In this scheme, the stroke period was divided into $N-1$ evenly spaced segments, the endpoints of which were the N nodes corresponding to the times of the discrete solution. The constraint in Eq. 6.1 was satisfied as

$$\frac{\mathbf{x}_{i+1}-\mathbf{x}_i}{h}-\mathbf{f}(\mathbf{x}_{av},\mathbf{u}_{av})=0 \tag{6.12}$$

where h is the time step, $h=t_{i+1}-t_i$ and $\mathbf{x}_{av}$ and $\mathbf{u}_{av}$ are the average values of the state and control variables over the time step. The end constraints $\psi(x_0,x_f,\dot{x}_0,\dot{x}_f)=0$ require that the derivative of the states also be equal at the beginning and end of the stroke. Because collocation does not allow for exact determination of the state and control derivatives at the nodes the end constraints were not satisfied in terms of $\psi(x_0,x_f,\dot{x}_0,\dot{x}_f)=0$, but by connecting the last and first nodes by a segment of length h. The constraints in Eq. 6.1 were enforced across this segment in the form

of Eq. 6.12 with node $i+1$ as node 1 and node i as node N. This can be viewed as completing the cycle of the stroke.

This method was not used throughout the project for many reasons. In classical collocation, many nodes are required to obtain a good solution which corresponds to many optimization parameters to be solved for. Because of the uniform distribution of the discretization nodes, this method is susceptible to the Runge phenomenon, or the divergence of the solution at the end points of the domain. It is also of great importance that the first derivative of the solution be known exactly at the nodes of discretization for tracking purposes, this method does not allow for this. For these reasons, a Chebyshev Pseudospectral Method is used for discretization of the OCP.

2. Chebyshev pseudospectral discretization

The Chebyshev Pseudospectral method as presented in [28], was used to convert the OCP in Sec. A to an NLP. This method was chosen primarily because it allows for exact determination of the state and control derivatives at the node points. This solution method also requires less node points and the distribution of these node points is such that the Runge phenomenon is prevented. These node points are those corresponding to the extrema of the Nth-order Chebyshev polynomial and are given analytically by

$$t_k = \cos(\frac{\pi k}{n}) \qquad k = 0, \ldots, n \tag{6.13}$$

The goal is to obtain a polynomial approximation of the solution in the following form,

$$\mathbf{x}^n(t) = \sum_{j=0}^{n} \mathbf{x}_j \phi_j(t), \tag{6.14}$$

$$\mathbf{u}^n(t) = \sum_{j=0}^{n} \mathbf{u}_j \phi_j(t), \tag{6.15}$$

where $\phi(t)$ are the Lagrange interpolating polynomials of order n. From its interpolating property, it can be shown [28] that

$$\mathbf{x}^n(t_k) = \mathbf{x}_k, \tag{6.16}$$

$$\mathbf{u}^n(t_k) = \mathbf{u}_k. \tag{6.17}$$

From this, it can be shown that the derivative of the $\mathbf{x}_k$ and $\mathbf{u}_k$ can be represented by a differentiation matrix times the state and control histories.

$$\dot{\mathbf{x}}^n(t_k) = \sum_{j=0}^{n} D_{kj} \mathbf{x}_j, \tag{6.18}$$

$$\dot{\mathbf{u}}^n(t_k) = \sum_{j=0}^{n} D_{kj} \mathbf{u}_j, \tag{6.19}$$

where D is $(N \times N)$ and N is the number of nodes, $N = n + 1$. The matrix D is computed from [28]. The differentiation matrix is multiplied by the vector of discrete values of each state variable to obtain the derivatives of those states at the node points.

3. Numerical computation

After the problem is discretized in time, a standard minization solver can be used to solve for the state and control histories. The solver used here is the FMINCON solver provided in the MATLAB optimization tool kit [29].

The FMINCON routine allows for linear and nonlinear path constraints as well as explicit upper and lower bounds on all parameters. Here we use the ability to enforce upper and lower bounds on the orientation of the wings. We use the nonlinear constraint feature to enforce the eight state evolution equations at the nodes. The nonlinear equality constraints are input in the following form

$$\mathbf{c}_{eq} = 0 \tag{6.20}$$

where $\mathbf{c}_{eq}$ is a vector that includes Eq. 6.1 satisfied at each node, as well as the periodic solution constraints in Eqs. 6.8 and 6.9. The nonlinear inequality constraints of Eqs. 6.3 or 6.10 are enforced similarly as

$$\begin{aligned} \mathbf{c} &= |\alpha_{eff}| - \alpha_{eff} && (6.21) \\ &\leq 0 && (6.22) \end{aligned}$$

where the vector $\mathbf{c}$ is of length N. The cost function in Eq. 6.5, is computed using a simple trapezoidal method. The inputs into FMINCON are the cost function evaluation routine, the constraint function evaluation routine, the upper and lower bounds on the states and controls constituting the trajectory and the initial guess

solution. The state and control history matrix is of the form

$$[\mathbf{x}] = \begin{bmatrix} \omega_1' & \theta_1' & \mathbf{u}_1' & \mathbf{V}(1)_1 & \mathbf{V}(3)_1 \\ \vdots & \vdots & \vdots & \vdots & \vdots \\ \omega_N' & \theta_N' & \mathbf{u}_N' & \mathbf{V}(1)_N & \mathbf{V}(3)_N \end{bmatrix} \tag{6.23}$$

where the prime denotes the transpose and the subscripts 1 and N denote the initial and final values of the state or control.

CHAPTER VII

AVIAN EXAMPLE

A. The Barn Swallow

A Barn Swallow was chosen as the example vehicle for demonstrating this method of designing a flapping wing vehicle wing stroke. This bird was chosen in part because of its size, it has a total wing span of 0.33m and a weight of approximately 0.20N.

Generally, the micro air vehicle class of vehicles is said to have a total wing span of less than or equal six inches, half that of the Barn Swallow. However, this method is intended to simplify the problem of designing a flapping wing stroke as much as possible while still retaining most of the useful substance of the problem. That is, the wing stroke optimization subject to vehicle and wing dynamics is retained. To this end, an example vehicle was desired that would have fairly low aspect wings so as not to invalidate the rigid wing assumption. However, the shorter the wings are, the less accurate are the aerodynamic assumptions. Considering this tradeoff, and the availability of the necessary data, the Barn Swallow seemed a reasonable choice. In the future, it may be desirable to consider a bird with available in flight wind tunnel data such as stroke period, stroke orientation history, power consumption data, etc..

From [30], preliminary values for many relevant quantities are found. Properties such as vehicle weight, wing area, wing span, cruise and minimum decent velocities. From these, the quantities finesse, or lift to drag ratio, wing aspect ratio, and non-dimensional parasite drag coefficient are extracted. Other parameters, such as the ratio of the wing mass to the fuselage mass, the wing moments of inertia, zero angle

of attack non-dimensional lift and the Oswald efficiency of the wing were assumed. These values are listed in Table I. It is desired to find an expression for parasite drag. Approximately, for trim,

$$\frac{L}{D} = \frac{U}{w} \tag{7.1}$$

$$\frac{C_L}{C_D} = \frac{U}{w} \tag{7.2}$$

from [30]. Where a U denotes forward velocity and w denotes downward velocity. We then enforce the $L = mg$ trim constraint and plug in Eq. 5.1

$$C_L = \frac{mg}{Q(2S)} \tag{7.3}$$

Also from [30], a decent ratio is used and from Eq. 7.2, the finesse is $F = 10$. Using the finesse in Eq. 7.2 and then substituting in Eqs. 7.3 and Eq. 5.7, the following is obtained

$$\frac{C_L}{C_D} = F \tag{7.4}$$

$$C_D = \frac{C_L}{F} \tag{7.5}$$

$$C_{D_0} + RC_L^2 = \frac{mg}{FQ(2S)} \tag{7.6}$$

$$C_{D_0} = \frac{mg}{FQ(2S)} - R\left(\frac{mg}{Q(2S)}\right)^2 \tag{7.7}$$

The physical parameters of the system (e.g. mass, wing area, etc.) are presented in Table I.

Table I. System parameters

Parameter	**Value**	**Units**
ρ	1.223	kg/m^3
g	9.81	kg-m/s^2
m	0.0204	kg
m_1	$0.05m$	kg
T	$\frac{1}{6}$	s
N	21	nodes
Wing geometry		
mgc	0.07878	m
span (wing 1)	0.165	m
S	0.013	m^2
AR	2.0942	
Oswald-eff	0.8	
Aerodynamic properties		
C_{L_0}	0	
C_{D_0}	0.0123	
C_{L_α}	2.864	rad^{-1}
R	0.189	rad^{-1}
F $\left(\frac{L}{D}\right)$	10	

The values of the inertia matrices of the wings (about the wing CG) are

$$[I_{c_1}] = [I_{c_2}] = 10^{-5} \begin{bmatrix} 0.2314 & 0 & 0 \\ 0 & 0.0527 & 0 \\ 0 & 0 & 0.2842 \end{bmatrix} \text{kg} - \text{m}^2 \tag{7.8}$$

The values of the vectors pointing from the fuselage to the wing 1 and 2 mass centers in their respective frames are

$$\mathbf{d}_{c_1} = [0, 0.0825, 0]^T \text{m} \tag{7.9}$$

$$\mathbf{d}_{c_2} = [0, -0.0825, 0]^T \text{m} \tag{7.10}$$

And the values of the wing 1 and 2 mgc quarter chord vectors are

$$\mathbf{d}_{q_1} = [-0.0197, 0.0825, 0]^T \text{m} \tag{7.11}$$

$$\mathbf{d}_{q_2} = [-0.0197, -0.0825, 0]^T \text{m} \tag{7.12}$$

These vectors specify the location of the aerodynamic center of each wing in the wing fixed frame. This is the point where the lift and drag are said to act and this is the vector that is used in the cross product to determine the aerodynamic moment on the wing.

These parameters are meant to approximate those associated with a common Barn Swallow [30], an aerobatic bird with a wing area, mass and wing span approximately equal to that mentioned above. The velocity of $V_r = 8\text{m/s}$ is the approximate

cruise speed of this bird. The frequency of the stroke is chosen as 6Hz. This wing beat frequency is chosen based on the advance ratio of the vehicle. The advance ratio of a flapping wing vehicle in trimmed flight is defined as

$$RA = \frac{\| \mathbf{V} \| T}{2span} \tag{7.13}$$

From data presented in [4], the advance ratio of small birds may vary between $RA = 1.61$ and $RA = 4.04$. From this, the period of the wing stroke is chosen to be $T = 1/6$s, which results in an advance ratio of about $RA = 4$.

B. Gliding flight

Gliding flight is an important mode of flight for many flapping wing vehicles. Gliding is the least expensive way for an air vehicle to travel in that it represents flight without the thrust force. Because there is no thrust force, the only force that counteracts the resistance of drag is gravity. The gliding mode of flight also represents trim for the dynamic system,

$$\dot{\mathbf{x}} = 0 \tag{7.14}$$

Trim is a very important concept in aircraft stability and control. In this section, the gliding mode of this type of flapping wing vehicle is investigated, stability characteristics are presented in Chapter IX.

1. Gliding state

When considering the glide trajectory of the vehicle in Chapter IV, the development begins with

$$\begin{bmatrix} \dot{\mathbf{V}}_p \\ \dot{\omega} \\ \dot{\theta} \end{bmatrix} = 0 \tag{7.15}$$

From the kinematics in Eq. 3.6 and the trim definition in Eq. 7.15, the angular velocity of the wings for this trim state will equal zero. The trim velocity of the vehicle and the trim orientation of the wings will have to be solved for to find a trim state. When Eq. 7.15 is substituted into Eqs. 4.21 and 4.34, the following is obtained,

$$\sum \mathbf{F}_A + m\mathbf{g} = 0 \tag{7.16}$$

$$\mathbf{u}_1 + \mathbf{M}_{A_1} = 0 \tag{7.17}$$

This is the familiar static force and moment balance. It says that the aerodynamic forces in the upward direction, the vehicle lift, must be equal and opposite the weight of the vehicle and that, for trim, the control moments are equal and opposite the applied aerodynamic moments on the wing. However, Eqs. 7.16 and 7.17 represent the total force balance on the vehicle and the moment balance on a single wing. For trim to be satisfied, the sum of all moments about the center of mass of the entire vehicle must be equal to zero. This yields the additional constraint

$$\sum \mathbf{M}_{CG} = 0, \tag{7.18}$$

where

$$\sum \mathbf{M}_{CG} = \mathbf{r}_{ac} \times \mathbf{F}_A \tag{7.19}$$

and

$$\mathbf{r}_{ac} = \frac{1}{2}(\mathbf{d}_{q_1} + \mathbf{d}_{q_2}) - \frac{1}{m}(m_1\mathbf{d}_{c_1} + m_2\mathbf{d}_{c_2}) \tag{7.20}$$

The quantity $\mathbf{r}_{ac}$, is the vector from the center of mass to the total aerodynamic center of the aircraft. The aerodynamic center of the aircraft is found from averaging the aerodynamic centers of the wings. Solving for a trim state can be done by posing an optimization problem of minimizing the scalar product of the total moments on the vehicle CG subject to the constraints in Eqs. 7.16 and 7.17. This problem is stated as such,

$$\min_{\rho} J$$

subject to the constraints of Eqs. 7.16 and 7.17, where the scalar cost function in this case is

$$J = [\mathbf{M}_{CG}]^T[\mathbf{M}_{CG}], \tag{7.21}$$

and the parameter vector of the optimization is

$$\rho = [\gamma, \theta_1, \theta_2, u_1, u_2, u_3]^T, \tag{7.22}$$

or

$$\rho = [\gamma, \theta_2, \theta_3, u_1, u_2, u_3]^T. \tag{7.23}$$

Whether θ_1 or θ_3 is chosen as an optimization variable represents choosing either the wing sweep angle or the wing plunge angle to be fixed and the other two to be solved for in driving the sum of moments on the system to zero. For this optimization, there are five constraint equations and six optimization variables, this allows for the satisfaction of the constraints while simultaneously minimizing the cost. If the number of optimization variables were equal to the number of constraint equations, the problem would be equally constrained and there would be exactly one solution to the problem. In gliding flight the ratio between descent velocity and forward airspeed equals the ratio between the vehicle drag and the weight of the vehicle [30],

$$\frac{\mathbf{V}_{fp}\sin(\gamma)}{\mathbf{V}_{fp}\cos(\gamma)} = \frac{D\cos(\gamma)}{W}. \tag{7.24}$$

After substituting the lift equal to weight constraint of trim,

$$\frac{\mathbf{V}_{fp}\sin(\gamma)}{\mathbf{V}_{fp}\cos(\gamma)} = \frac{D\cos(\gamma)}{L\cos(\gamma)}, \tag{7.25}$$

which leads to,

$$\tan(\gamma) = \frac{D}{L}. \tag{7.26}$$

If it is assumed that γ is small,

$$\gamma = \frac{D}{L}. \tag{7.27}$$

The convention used here is that a positive γ rotation is upward, thus

$$\gamma \ = -\tfrac{D}{L} \ = -\frac{1}{F}. \tag{7.28}$$

For this simple case of zero sweep and zero plunge, the equilibrium pitch attitude of the wings is a linear combination of the flight path angle and the angle of attack. To find the trim angle of attack, the known lift to drag ratio of the vehicle and the lift equal to weight constraint of trim are used. This begins with the equation for lift,

$$L = Q(2S)C_L, \tag{7.29}$$

where the dynamic pressure is a function of the vehicle velocity, $Q = 1/2\rho V_{fp}^2$. The α_{eff} in Eq. 5.6 is only a function of the forward velocity of the vehicle in gliding flight and is solved for next. Substituting Eq. 5.6 into Eq. 7.29, the following is obtained,

$$L = Q(2S)(C_{L_0} + C_{L_\alpha}\alpha_{tr}), \tag{7.30}$$

$$mg = Q(2S)(C_{L_0} + C_{L_\alpha}\alpha_{tr}), \tag{7.31}$$

rearranging,

$$\alpha_{tr} = \frac{mg}{2QSC_{L_\alpha}} - \frac{C_{L_0}}{C_{L_\alpha}}. \tag{7.32}$$

From Eqs. 7.28 and 7.32, the trim flight path angle and trim angle of attack of the vehicle, and with the plunge and sweep angles equal zero, the angle of attack can be found from the relationship,

$$\alpha = \theta(2) - \gamma, \tag{7.33}$$

where $\theta(2)$ is the pitch attitude. From this, the expression for the trim pitch attitude of the wing, for the zero sweep, zero plunge case is,

$$\theta_{tr}(2) = \alpha_{tr} + \gamma_{tr}. \tag{7.34}$$

The trim value of the inertial velocity of the vehicle is found from Eq. 7.28 and the chosen flight path velocity. The trim value of the wing orientation is known from Eq. 7.34. The aerodynamic moments on the wing are be solved for using Eqs. 5.6-5.12 and the trim values of the states. And from Eq. 7.17, the equilibrium values of the controls are found. While this approximation gets fairly close to the solution to the nonlinear algebraic trim equations 7.16, 7.17, this solution does not satisfy the constraint that the moments on the system be zero. It is desirable to use the afore mentioned optimization scheme to solve for a trim that satisfies the constraints of Eqs. 7.16 and 7.17 while achieving zero moments on the system. The Matlab function 'FMINCON' [29], is used to numerically solve the trim optimization problem, accepting the above solution as an initial guess.

2. Linearization about trim

The linearization of the model of the system about a trim state is discussed here. Ultimately, the inertial velocity of the vehicle is to be controlled. It will be useful to get a sense of the stability of the velocity states when the orientation of the wings is used as the control instead of the control moments. For this analysis, the states for the new system are chosen as

$$\mathbf{x} = \begin{bmatrix} \mathbf{V}(1) \\ \mathbf{V}(3) \end{bmatrix}, \tag{7.35}$$

and the controls, instead of the applied moments at the root of the wing, are the Euler Angles of the individual wing,

$$\mathbf{u} = \theta. \tag{7.36}$$

Choosing the wing orientation as the control for the system is analogous to choosing the elevator on an airplane as the longitudinal control. This setup assumes that the orientation of the wing is commanded instantaneously. To analyze the stability of the resulting system, the translational equations of motion must be in the form,

$$\dot{\mathbf{x}} = [A]\mathbf{x} + [B]\mathbf{u}. \tag{7.37}$$

Eq. 4.21 are the full translational equations of motion for the fuselage of the vehicle. Eq. 4.21 represents a set of three nonlinear equations. The first and third of these equations describe the longitudinal motion of the vehicle fuselage. The second

one is a constraint on the velocity perpendicular to the longitudinal plane and equals zero for all time. This is satisfied by the symmetry relationship in Eq. 3.3. Only the first and third of Eq. 4.21 will be used. Finding the linearized equations Eq. 7.37 begins with providing a point to linearize about. While an equilibrium point of the nonlinear system is often a desirable point to ascertain stability characteristics about, linearizing about a trajectory that the nonlinear system is to track could also be desirable. The Simulink function 'linmod' is used to linearize the translational dynamics and obtain $[A]$ and $[B]$ in Eq. 7.37. The inputs to this function are the equations of motion and the values of the states and controls that the system is to be linearized about, the equilibrium point.

CHAPTER VIII

CONTROLLER DESIGN

This chapter discusses the design of a controller that is used to track gliding and flapping reference trajectories. The controller is designed using a dynamic inversion scheme [31]. Dynamic inversion is a technique that incorporates the knowledge of model kinematics and dynamics in order to achieve asymptotic tracking for dynamical systems. This controller allows the cancellation of the nonlinear dynamics of the problem and replacement with a stable, linear dynamics that are guaranteed to converge to the desired reference trajectory. The stability of the controller is proved using a Lyapunov stability analysis [31].

A. Tracking controller

This system is under-actuated, the number of controls is less that the number of degrees of freedom. The only controls in the system are the actuators at the root of the wings that apply the control moments $\mathbf{u}$. Because only the motions of one wing are considered, their are three independent controls. However, there are five acceleration level equations of motion and five degrees of freedom. These five equations are coupled at the acceleration level. This coupling is handled through substitution of the translational dynamics into the rotational dynamics which eliminates the fuselage acceleration from the rotational dynamics. The rotational dynamics are then considered to be controlled independently with knowledge of the instantaneous translational states. This results in a square, invertible control influence matrix allowing

for an easier control design task. The stability of the closed loop system is proved using a Lyapunov function, this is an energy-like function that is a function of the states of the system, or in this case, the error between the tracking states and the reference to be tracked. This function must be positive semi-definite and radially unbounded for all values of the error and its derivative must be negative for all values of the errors. Intuitively, this means that the error energy of the system must always decrease unless at zero. It is shown that the controller ensures the existence of such a function.

1. Error dynamics

One of the benefits of this type of controller is that the dynamics of the system are replaced with the dynamics desired by the control designer. It is often desirable to choose stable linear tracking error dynamics for the controller to enforce. This will ensure that the system state trajectories converge to the desired reference trajectories. The desired error dynamics that are used here are linear functions of the Euler angle errors and rates and are

$$\ddot{\mathbf{e}} + C\dot{\mathbf{e}} + K\mathbf{e} = 0. \tag{8.1}$$

The matrices C and K are symmetric, positive definite gain matrices that are used to tailor the error dynamics. The error dynamics in Eq. 8.1 are asymptotically stable and if imposed, will cause the attitude error, $\mathbf{e}$, to decay to zero. The attitude error, $\mathbf{e}$, is defined as

$$\mathbf{e} = \theta - \theta_r. \tag{8.2}$$

This attitude error does not represent the relative attitude of the reference frame to the 1-frame, however, when $\mathbf{e}$ goes to zero, the body frame and the 1-frame have the same orientation relative to the inertial frame. From Eq. 3.6, we have the kinematics of the 1-frame,

$$\dot{\theta} = \mathbf{f}(\theta, \omega), \tag{8.3}$$

$$= A(\theta)\omega, \tag{8.4}$$

upon differentiating,

$$\ddot{\theta} = \frac{\delta \mathbf{f}}{\delta \theta}\dot{\theta} + \frac{\delta \mathbf{f}}{\delta \omega}\dot{\omega}. \tag{8.5}$$

Because the intent here is to track only the wing attitude and the associated rates, the equation of motion of the wing must have only acceleration level kinematics of the wing and not contain the vehicle translational acceleration. To this end, the translational acceleration equation of the vehicle is substituted into the rotational equation of motion of the wing to obtain the wing 1 equation of motion in the following structure,

$$\dot{\omega} = \mathbf{g}(\theta, \omega, \mathbf{V}_p) + [h(\theta)]\mathbf{u}. \tag{8.6}$$

Substituting Eq. 8.6 into Eq. 8.5,

$$\ddot{\theta} = \frac{\delta \mathbf{f}}{\delta \theta}\dot{\theta} + \frac{\delta \mathbf{f}}{\delta \omega}\mathbf{g}(\theta, \omega, \mathbf{V}_p) + \frac{\delta \mathbf{f}}{\delta \omega}[h(\theta)]\mathbf{u}. \tag{8.7}$$

Eq. 8.7 is then substituted into Eq. 8.1 to eliminate $\ddot{\theta}$ from the error dynamics. This is done so that the acceleration level attitude kinematics do not have to be feedback to the controller. The new error dynamics are

$$\frac{\delta \mathbf{f}}{\delta \theta}\dot{\theta} + \frac{\delta \mathbf{f}}{\delta \omega}\mathbf{g}(\theta, \omega, \mathbf{V}_p) + \frac{\delta \mathbf{f}}{\delta \omega}[h(\theta)]\mathbf{u} - \ddot{\theta}_r + C\dot{\mathbf{e}} + K\mathbf{e} = 0. \tag{8.8}$$

The function $(\delta \mathbf{f}/\delta \omega)[h(\theta)]$ must be invertable in order to solve Eq. 8.8 for the control input. The control input is

$$\mathbf{u} = -\left[\frac{\delta \mathbf{f}}{\delta \omega}[h(\theta)]\right]^{-1}\left(\frac{\delta \mathbf{f}}{\delta \theta}\dot{\theta} + \frac{\delta \mathbf{f}}{\delta \omega}\mathbf{g}(\theta, \omega, \mathbf{V}_p) + \frac{\delta \mathbf{f}}{\delta \omega} - \ddot{\theta}_r + C\dot{\mathbf{e}} + K\mathbf{e}\right). \tag{8.9}$$

This controller will achieve asymptotic tracking for the system. The proof of the asymptotic stability of the controller follows.

2. Lyapunov stability analysis of controller

Lyapunov's theorem for global stability states that if there exists a scalar function V_L of the states $\mathbf{x}$, with continuous first order derivatives such that

$V_L(\mathbf{x})$ *is positive definite*,

$\dot{V}_L(\mathbf{x})$ *is negative definite*,

$V_L(\mathbf{x}) \rightarrow \infty$ *as* $\| \mathbf{x} \| \rightarrow \infty$,

then the equilibrium point at the origin is globally asymptotically stable [32]. Qual-

itatively, this can be compared to the energy of the system. Consider a simple spring-mass-damper system, the energy of the system is always positive except when the position and velocity are zero. With the damper in place the system energy is monotonically decreasing. While the energy equation of a system does not always provide a suitable Lyapunov function, the principle is the same.

The Lyapunov function used is

$$V_L(\mathbf{e}, \dot{\mathbf{e}}) = \frac{1}{2}\dot{\mathbf{e}}^T\dot{\mathbf{e}} + \frac{1}{2}\mathbf{e}^T K\mathbf{e}. \tag{8.10}$$

This is a positive semi-definite function of the orientation error and orientation error rate. It is zero only when both are zero. This can be considered to be the error energy of the rotational part of the system. The derivative of this Lyapunov function is

$$\dot{V}_L = \dot{\mathbf{e}}^T\ddot{\mathbf{e}} + \dot{\mathbf{e}}^T K\mathbf{e} \tag{8.11}$$

To show that $\dot{V}_L$ is negative definite, the error dynamics from Eq. 8.1, that are enforced by the control law are substituted into Eq. 8.11. The following is obtained,

$$\begin{aligned} \dot{V}_L &= \dot{\mathbf{e}}^T(-C\dot{\mathbf{e}} - K\mathbf{e} + K\mathbf{e}) && (8.12)\\ &= -\dot{\mathbf{e}}^T C\dot{\mathbf{e}} && (8.13) \end{aligned}$$

Eq. 8.13 is clearly negative for all $\dot{\mathbf{e}}$ greater than zero. However, because $\dot{\mathbf{V}}_L$ is only negative semi-definite, another method must be used to prove asymptotic stability. If the next odd derivative of V_L, $\dddot{V}_L < 0, \forall \mathbf{e} \neq 0$ on a set, $\mathrm{S}\{\dot{\mathbf{e}} = 0, \mathbf{e} = \Re\}$,

then the system is asymptotically stable [33].

$$\ddot{V}_L = -2\ddot{\mathbf{e}}^T C\dot{\mathbf{e}}. \tag{8.14}$$

The third derivative of V_L is

$$\begin{aligned} \dddot{V}_L &= -2\dddot{\mathbf{e}}^T C\dot{\mathbf{e}} - 2\ddot{\mathbf{e}}^T C\ddot{\mathbf{e}}, & (8.15)\\ &= -2\dddot{\mathbf{e}}^T C\dot{\mathbf{e}} - 2(-C\dot{\mathbf{e}} - K\mathbf{e})^T C(-C\dot{\mathbf{e}} - K\mathbf{e}). & (8.16) \end{aligned}$$

Upon defining $\dddot{V}_L$ on the set S, the following is obtained,

$$\dddot{V}_L = -2\mathbf{e}^T K^T CK\mathbf{e} \tag{8.17}$$

The matrix $K^T CK$ is positive definite, thus $\dddot{V}_L < 0, \forall \mathbf{e} \neq 0$ on S.

However, this is not a Lyapunov function for the system. It is only a function of the wing orientation and orientation rate errors. Thus, this analysis only guarantees asymptotic tracking for the angular orientation and orientation rates. From the orientation kinematics in Eq. 3.6, if $\theta \to \theta_r$ and $\dot{\theta} \to \dot{\theta}_r$ then $\omega \to \omega_r$. This control strategy guarantees asymptotic tracking for the Euler Angles, angular velocities and angular velocity rates. From the dynamics in Eq. 8.6, if the rotational kinematics converge to the reference values, because Eq. 8.6 is also a function of the velocity states, the translational velocities must also converge to values consistent with Eq. 8.6. For nonlinear systems in general, there can be more than one equilibrium point, but for this analysis, it is assumed that the system operates sufficiently close to the equilibrium that corresponds to the reference velocities generated by the wing stroke

optimization. This convergence is seen in simulation.

3. The controller

The above controller is a nonlinear dynamic inversion controller that cancels out the nonlinear dynamics of the physical system and replaces the undesired dynamics with the dynamics in Eq. 8.1. However, the controller in Eq. 8.9 requires complete knowledge of the system dynamics, Eqs. 4.21 and 4.34 which, in practice are not known precisely. This controller also has no mechanism for coping with actuator saturation of any kind. In practice, all actuators have limits on the control effort that can be exerted and the rate at which that control effort can be changed. Along with these traits, real actuators have internal dynamics associated with their operation. Actuator dynamics are not considered in this analysis. The controller in Eq. 8.9 is restated here for convenience.

$$\mathbf{u} = -\left[\frac{\delta \mathbf{f}}{\delta \omega}[h(\theta,\omega)]\right]^{-1}\left(\frac{\delta \mathbf{f}}{\delta \theta}\dot{\theta} + \frac{\delta \mathbf{f}}{\delta \omega}\mathbf{g}(\theta,\omega) + \frac{\delta \mathbf{f}}{\delta \omega} - \ddot{\theta}_r + C\dot{\mathbf{e}} + K\mathbf{e}\right). \tag{8.18}$$

The partial derivatives, $\delta\mathbf{f}/\delta\theta$ and $\delta\mathbf{f}/\delta\omega$, of the vector function $\mathbf{f}$ are the partial derivatives of Eq. 3.6 and are,

$$\frac{\delta \mathbf{f}}{\delta \theta} = \left[\frac{\delta \mathbf{f}}{\delta \theta_1}, \frac{\delta \mathbf{f}}{\delta \theta_2}, \frac{\delta \mathbf{f}}{\delta \theta_3}\right], \tag{8.19}$$

where the subscripts $1, 2, 3$ denote the $1, 2$ and 3 rotations of the 1-frame and

$$\frac{\delta \mathbf{f}}{\delta \theta_1} = \frac{1}{c\theta_2} \begin{bmatrix} 0 & s\theta_2 c\theta_1 & -s\theta s\theta_1 \\ 0 & -c\theta_2 s\theta_1 & -c\theta_2 c\theta_1 \\ 0 & c\theta_1 & -s\theta_1 \end{bmatrix}, \tag{8.20}$$

$$\frac{\delta \mathbf{f}}{\delta \theta_2} = -\frac{1}{c\theta_2} \left(\frac{1}{c\theta_2} \begin{bmatrix} c\theta_2 & s\theta_2 s\theta_1 & s\theta_2 c\theta_1 \\ 0 & c\theta_2 c\theta_1 & -c\theta_2 s\theta_1 \\ 0 & s\theta_1 & c\theta_1 \end{bmatrix} - \begin{bmatrix} -s\theta_2 & c\theta_2 s\theta_1 & c\theta_2 c\theta_1 \\ 0 & -s\theta_2 c\theta_1 & s\theta_2 s\theta_1 \\ 0 & 0 & 0 \end{bmatrix} \right) \omega, \tag{8.21}$$

$$\frac{\delta \mathbf{f}}{\delta \theta_3} = \mathbf{0}, \tag{8.22}$$

and the partial derivative of $\mathbf{f}$ with respect to the angular velocity of the wing is

$$\frac{\delta \mathbf{f}}{\delta \omega} = [A(\theta)]. \tag{8.23}$$

The vector and matrix functions $\mathbf{g}(\theta, \omega, \mathbf{V}_p)$ and $[h(\theta)]$ in Eq. 8.6 are nonlinear functions of the states and include the velocity states. The substitution performed to obtain these functions is as follows, the two vector equations of motion are restated here for convenience.

$$\begin{aligned} m\frac{^i d}{dt}(\mathbf{V}_p) - (m_1[\mathbf{d}_{c_1}^{\times}]\dot{\omega}_1 + m_2[\mathbf{d}_{c_2}^{\times}]\dot{\omega}_2) \\ + (m_1[\omega_1^{\times}]^2\mathbf{d}_{c_1} + m_2[\omega_2^{\times}]^2\mathbf{d}_{c_2}) = \sum \mathbf{F}_A + m\mathbf{g} \end{aligned} \tag{8.24}$$

and

$$(I_1 - m_1[\mathbf{d}_{c_1}^{\times}]^2)\dot{\omega}_1 + [\omega_1^{\times}](I_1 - m_1[\mathbf{d}_{c_1}^{\times}]^2)\omega_1 + m_1[\mathbf{d}_{c_1}^{\times}]\frac{^i d}{dt}(\mathbf{V}_p) = \mathbf{u}_1 + \mathbf{M}_{A_1} \tag{8.25}$$

are the equations governing the evolution of the fuselage velocity and wing angular velocity respectively. The expression for the angular velocity rate that is independent of the velocity rate is sought here. In preparation for substitution, Eq. 8.24 is rearranged as

$$\begin{aligned}\frac{^i d}{dt}(\mathbf{V}_p) = \frac{1}{m}(\sum \mathbf{F}_A + m\mathbf{g} + (m_1[\mathbf{d}_{c_1}^{\times}]\dot{\omega}_1 + m_2[\mathbf{d}_{c_2}^{\times}]\dot{\omega}_2) \\ - (m_1[\omega_1^{\times}]^2\mathbf{d}_{c_1} + m_2[\omega_2^{\times}]^2\mathbf{d}_{c_2})).\end{aligned} \tag{8.26}$$

With this and through the use of the symmetry relationship in Eq. 3.16, the following form of Eq. 8.25 is obtained.

$$\begin{aligned}[I_1 - m_1[\mathbf{d}_{c_1}^{\times}]^2 + \frac{m_1 m_1}{m}[\mathbf{d}_{c_1}^{\times}][\mathbf{d}_{c_1}^{\times}] + \frac{m_1 m_2}{m}[\mathbf{d}_{c_1}^{\times}][\mathbf{d}_{c_2}^{\times}][T]]\dot{\omega}_1 = \mathbf{u}_1 + \mathbf{M}_{A_1} \\ - [\omega_1^{\times}](I_1 - m_1[\mathbf{d}_{c_1}^{\times}]^2)\omega_1 \\ - \frac{m_1}{m}[\mathbf{d}_{c_1}^{\times}](\sum \mathbf{F}_A + m\mathbf{g} - m_1[\omega_1^{\times}]^2\mathbf{d}_{c_1} - m_2[\omega_2^{\times}]^2\mathbf{d}_{c_2}).\end{aligned} \tag{8.27}$$

From Eq. 8.27, it is apparent that $\mathbf{g}(\theta, \omega, \mathbf{V}_p)$ and $[h(\theta)]$ in Eq. 8.6 are

$$\begin{aligned}\mathbf{g}(\theta, \omega, \mathbf{V}_p) = &[I_1 - m_1[\mathbf{d}_{c_1}^{\times}]^2 + \frac{m_1 m_1}{m}[\mathbf{d}_{c_1}^{\times}][\mathbf{d}_{c_1}^{\times}] + \frac{m_1 m_2}{m}[\mathbf{d}_{c_1}^{\times}][\mathbf{d}_{c_2}^{\times}][T]]^{-1} \\ &(\mathbf{M}_{A_1} - [\omega_1^{\times}](I_1 - m_1[\mathbf{d}_{c_1}^{\times}]^2)\omega_1 \\ &- \frac{m_1}{m}[\mathbf{d}_{c_1}^{\times}](\sum \mathbf{F}_A + m\mathbf{g} - m_1[\omega_1^{\times}]^2\mathbf{d}_{c_1} - m_2[\omega_2^{\times}]^2\mathbf{d}_{c_2}))\end{aligned} \tag{8.28}$$

and

$$[h(\theta)] = [I_1 - m_1[\mathbf{d}_{c_1}^{\times}]^2 + \frac{m_1 m_1}{m}[\mathbf{d}_{c_1}^{\times}][\mathbf{d}_{c_1}^{\times}] + \frac{m_1 m_2}{m}[\mathbf{d}_{c_1}^{\times}][\mathbf{d}_{c_2}^{\times}][T]]^{-1} \tag{8.29}$$

Recall that the error between the actual velocity and the velocity that corresponds to the optimized wing stroke is not included in the error dynamics or the Lyapunov function and thus there is no stability guarantee associated with the translational velocity states. The velocity states are however, coupled to the other states and thus effect the equilibrium of the system.

B. Reference trajectory generation

The solution to the discretized optimal control problem yields, for each state and control, a sequence of discrete values corresponding to predetermined time points along the period of the wing stroke. In order for the control to track the trajectory, the state trajectories must be continuous. A piecewise continuity can be obtained using polynomial fits between the optimized data points. The control law in Eq. 8.18 will track the reference orientations generated by the optimization routine. An expression is desired that, when given the values of the states and controls and the state and control rates at discrete times, will yield the values of the states and controls and their respective derivatives for a desired time in between.

The following notation will denote node i as the node at the discrete time point immediately preceding the current time and node $i + 1$ as the node corresponding to the time immediately following the current time point along the period of the

stroke. A Δt_i will denote the current time, or time at which the states and controls are desired along the interval between node i and node $i+1$. Here, $\Delta t = 0$ at node i and $\Delta t = \Delta t_f$ at node $i+1$, at the end of the interval. From the kinematics,

$$\dot{\theta}_i = [A_i(\theta_i)]\omega_i \tag{8.30}$$

$$\dot{\theta}_{i+1} = [A_{i+1}(\theta_{i+1})]\omega_{i+1} \tag{8.31}$$

and from the optimization, the discrete trajectory is

$$[\mathbf{x}_{traj}] = \begin{bmatrix} \mathbf{V}'_{p_1} & \omega'_1 & \theta'_1 \\ \vdots & \vdots & \vdots \\ \mathbf{V}'_{p_N} & \omega'_N & \theta'_N \end{bmatrix} \tag{8.32}$$

$$[\mathbf{u}_{traj}] = \begin{bmatrix} \mathbf{u}'_1 \\ \vdots \\ \mathbf{u}'_N \end{bmatrix} \tag{8.33}$$

The derivatives of the states and controls are given, as in Eqs. 6.18 and 6.19, by

$$\dot{\mathbf{x}}_{traj} = [D]\mathbf{x}_{traj}, \tag{8.34}$$

$$\dot{\mathbf{u}}_{traj} = [D]\mathbf{u}_{traj}. \tag{8.35}$$

A third order spline fit is used. The procedure for this type of interpolation will be discussed in the general context of a single scalar parameter, however, this

is readily extended to use with vectors. Here, the known values at the end points of the interpolation interval are the values of the function and its derivative. These are denoted as $q_i, \dot{q}_i, q_{i+1}, \dot{q}_{i+1}$. The polynomial fit is of the form

$$q(\Delta t) = a + b\Delta t + c\Delta t^2 + d\Delta t^3. \tag{8.36}$$

Using the end conditions of the parameter value and the derivative,

$$\begin{aligned}
q(\Delta t_i) = q_i &= a_i + b_i\Delta t_i + c_i\Delta t_i^2 + d_i\Delta t_i^3, && (8.37)\\
q(\Delta t_{i+1}) = q_{i+1} &= a_i + b_i\Delta t_{i+1} + c_i\Delta t_{i+1}^2 + d_i\Delta t_{i+1}^3, && (8.38)\\
\dot{q}(\Delta t_i) = \dot{q}_i &= b_i + 2c_i\Delta t_i + 3d_i\Delta t_i^2, && (8.39)\\
\dot{q}(\Delta t_{i+1}) = \dot{q}_{i+1} &= b_i + 2c_i\Delta t_{i+1} + 3d_i\Delta t_{i+1}^2. && (8.40)
\end{aligned}$$

These equations can be cast in matrix form as

$$\begin{bmatrix} 1 & \Delta t_i & \Delta t_i^2 & \Delta t_i^3 \\ 1 & \Delta t_{i+1} & \Delta t_{i+1}^2 & \Delta t_{i+1} \\ 0 & 1 & 2\Delta t_i & 3\Delta t_{i+1}^2, \\ 0 & 1 & 2\Delta t_{i+1} & 3\Delta t_{i+1}^2 \end{bmatrix} \begin{pmatrix} a_i \\ b_i \\ c_i \\ d_i \end{pmatrix} = \begin{pmatrix} q(\Delta t_i) \\ q(\Delta t_{i+1}) \\ \dot{q}(\Delta t_i) \\ \dot{q}(\Delta t_{i+1}) \end{pmatrix}. \tag{8.41}$$

The polynomial coefficients a, b, c and d are

$$\begin{pmatrix} a_i \\ b_i \\ c_i \\ d_i \end{pmatrix} = \begin{bmatrix} 1 & \Delta t_i & \Delta t_i^2 & \Delta t_i^3 \\ 1 & \Delta t_{i+1} & \Delta t_{i+1}^2 & \Delta t_{i+1} \\ 0 & 1 & 2\Delta t_i & 3\Delta t_{i+1}^2 \\ 0 & 1 & 2\Delta t_{i+1} & 3\Delta t_{i+1}^2 \end{bmatrix}^{-1} \begin{pmatrix} q(\Delta t_i) \\ q(\Delta t_{i+1}) \\ \dot{q}(\Delta t_i) \\ \dot{q}(\Delta t_{i+1}) \end{pmatrix}. \tag{8.42}$$

Once the coefficients corresponding to each reference state are determined, the interpolated value of all of the states and their rates can be found. These reference values are used in the tracking controller.

CHAPTER IX

DISCUSSION OF RESULTS

This chapter presents the results from wing stroke generation, linearization results in gliding flight, wing stroke tracking using the dynamic inversion controller, and translational stability analysis in flapping flight. Cases are presented that demonstrate the versatility of the stroke generation method, the gliding stability configurations of the vehicle and the convergent properties of the controller. The linearization results show the stability of the velocity states in gliding flight when the orientation of the wings is used as the control effecter. The translational stability analysis in flapping flight is a qualitative analysis of the stability of the velocity states in flapping flight.

A. Trajectory generation results

This section presents the results of the wing stroke generation method for three cases. The three cases are designed to demonstrate the ability of the method to design wing strokes that correspond to various longitudinal trim conditions. The first case is for a reference flight path velocity and angle of $8m/s$ and 0° respectively. This flight condition represents steady level flight at the cruise velocity of the vehicle [30]. In the second case, the reference flight path velocity and angle are $8m/s$ and 3° respectively, which corresponds to climbing flight at the cruise velocity. And the third case is for a reference flight path velocity and angle of 6m/s and 0°, this is a steady level flight condition with a velocity below the cruise velocity. Table II organizes some of the more pertinent results of the three optimizations. The major

Table II. Trajectory generation summary

Quantity	**Case 1**	**Case 2**	**Case 3**
V_r, m/s	8	8	6
γ_r,°	0	3	0
β_1	1	1	1
β_2	0.001	0.001	0.001
Max mgqc velocity, m/s	8.62	8.97	6.73
Min mgqc velocity, m/s	7.57	7.75	5.66
Average lift, N	0.2001	0.2001	0.2001
Reduced frequency, k_{max}	0.192	0.188	0.258
Advance ratio	4.02	4.13	3.03

parameters that determine the result of the optimization within the constraints are the reference flight path velocity (V_r) and angle (γ_r) and the relative weighting of the flight path angle error, flight path velocity error (β_1) and the control rate (β_2) in the cost function.

1. Case 1

Fig. 6 shows an inertial view of the wing orientation history. Consider the vehicle translating toward the right hand side of the figure. The curve ABC, in Fig. 6 represents the path of a point on the wing mean geometric chord at the leading edge of the wing. The intersecting lines represent the mgc over the stroke period. While this view is $2D$, the motion of the mgc is $3D$, however, this figure helps to

visualize the Euler angle orientation of the wing and get an inertial sense of the trajectory. The circle in Fig. 6 represents the fuselage and the wing mgc is plotted relative to the vehicle fuselage. This view is from the right wingtip looking down the wing. Fig. 6 is a view in a reference frame that does not rotate, but translates relative to the inertial frame. The point 'A' in Fig. 6 indicates the point where the maximum inertial velocity of the mean geometric quarter chord occurs. The point 'B' in Fig. 6 indicates the point where the minimum inertial velocity of the mean geometric quarter chord occurs. The point 'C' indicates the start and finish of the stroke. From Table II, the reduced frequencies are within the range where the phasing between the motion of the wings and the resulting aerodynamic loads becomes important [15]. However, these effects are not included here.

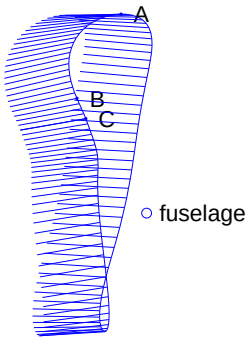

Fig. 6. Case 1. Wing stroke, inertial view from wing tip. This is the history of the wing mean geometric chord over the stroke period. Stroke is in clockwise direction.

Figs. 7(a)-7(c) present the fuselage flight path velocity, V_{fp}, flight path angle,

γ, and wing effective angle of attack, α_{eff}, time histories. Recall that the objective is to minimize the areas under the velocity, flight path angle and control rate curves with respect to the reference values. It is seen that the velocity and flight path angle stay fairly close to the their respective reference values as intended by the choice of cost function. The periodic nature of the vehicle motion can also be seen. Note that the angle of attack stays well within the bounds of $|\alpha_{eff}| \leq 20^{\circ}$. It is noted that the flight path angle and velocity both decrease at the start of the stroke. This is counter intuitive because fixed-wing aircraft flying at trim will generally trade velocity for an increase in flight path angle and altitude. Here however, the lift force, decreases at the start of the stroke and at the same time, there is a net drag, on the vehicle that result in the decrease of velocity and flight path angle. Because the lift and gravity forces primarily influence the flight path angle rate and gravity is dominant at the start of the stroke, the flight path angle decreases. The vehicle still experiences a parasite drag that causes the velocity to decrease as well.

Figs. 8(a)-8(c) show angular velocities, Euler angle kinematics and control trajectories corresponding to the above stroke. Note that all of the Euler angles stay well away from 90° and any kinematic singularities. Also from Fig. 8(b), it can be seen that the θ_1 Euler angle, or plunge history, is the one that most closely resembles a single sinusoid.

Figs. 9(a)-9(b) present the time histories of the total aerodynamic force on the vehicle in the inertial 1 and 3 directions respectively. Recall that gravity acts in the positive 3-direction. It can be seen that the force in the 3-direction closely follows the effective angle of attack in Fig. 7(c) as the lift is largely a function of α_{eff}.

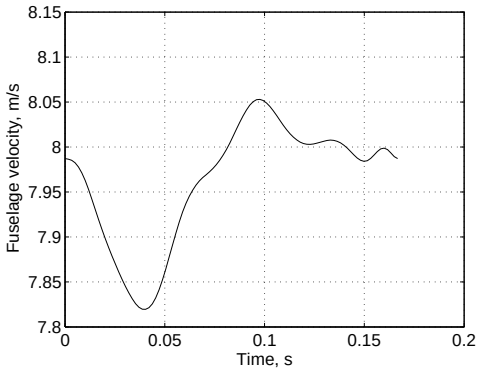

(a) Flight path velocity

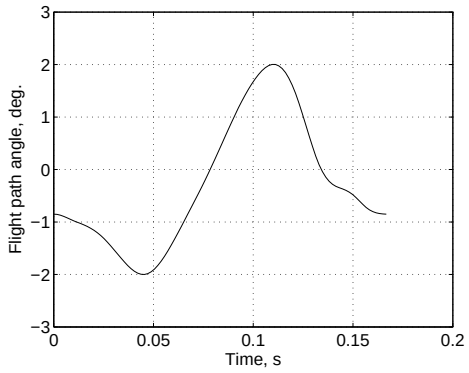

(b) Flight path angle

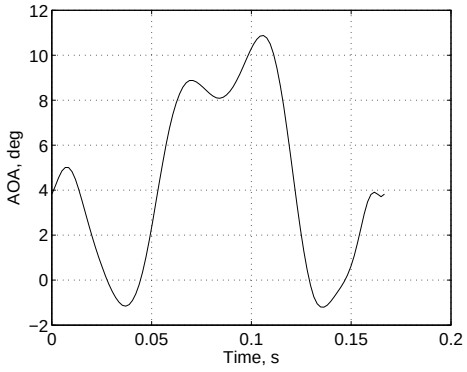

(c) Angle of attack

Fig. 7. Case 1. Velocity, flight path angle and effective angle of attack time histories.

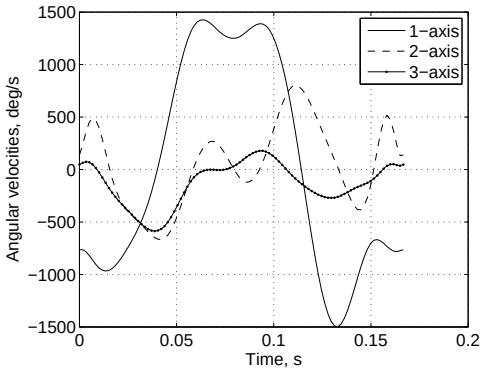

(a) Angular velocities

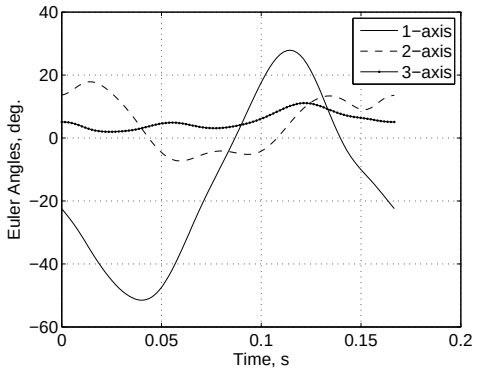

(b) Euler angle orientation

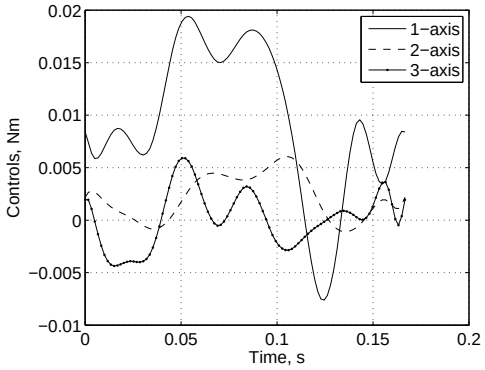

(c) Controls

Fig. 8. Case 1. Angular velocity, orientation and control time histories.

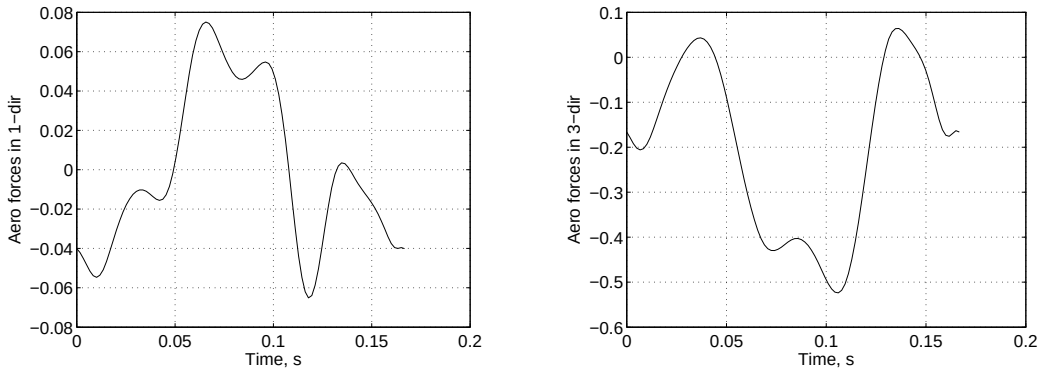

(a) Total aerodynamic force in inertial 1-direction

(b) Total aerodynamic force in inertial 3-direction

Fig. 9. Case 1. Total aerodynamic forces on the vehicle in the inertial frame. The forces in the 1-direction represent the balance of thrust and drag.

2. Case 2

The wing stroke generated for case 2 corresponds to a $\gamma_r = 3°$ and a $V_r = 8\text{m/s}$. It is shown here that the method can be used to design wing strokes that will maintain the vehicle at a near trim flight path angle other than 0°. A positive flight path angle is chosen because it represents climbing flight.

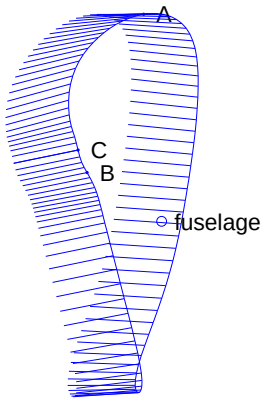

Fig. 10. Case 2. Wing stroke, inertial view from wing tip. This is the history of the wing mean geometric chord over the stroke period.

Notice the orientation of the wing relative to the fuselage for Case 2, Fig. 10. The leading edge of the wing transcribes a larger loop and is forward of the fuselage for more of the stroke. The velocity and flight path angle in Figs. 11(a) and 11(b) stay fairly close to their respective reference values.

The kinematics in Figs. 12(a) and 12(b) show a noticeable difference from those of Case 1. The sweep angle of the wings is not positive through the entire stroke. This can also be seen in Fig. 10 where the fuselage is farther behind the wing stroke

than in Fig. 6.

Figs. 13(a) and 13(b) show the aerodynamic forces on the vehicle for Case 2. The average of these force correspond to trim for the vehicle.

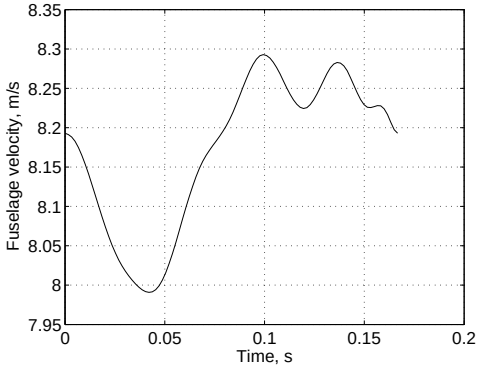

(a) Flight path velocity

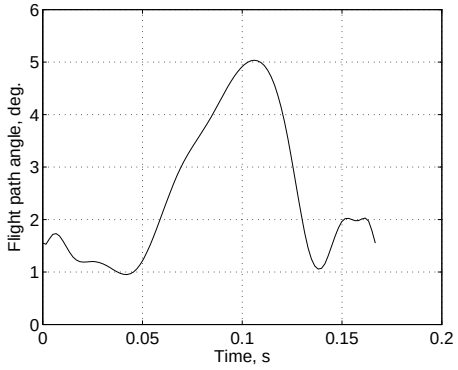

(b) Flight path angle

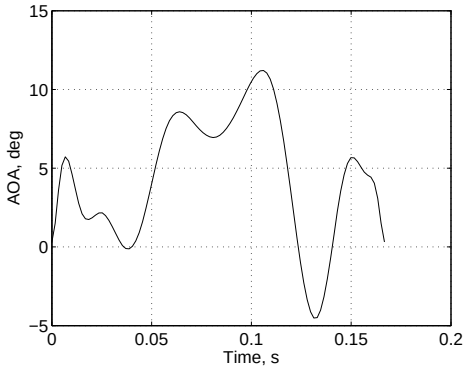

(c) Angle of attack

Fig. 11. Case 2. Velocity, flight path angle and effective angle of attack time histories.

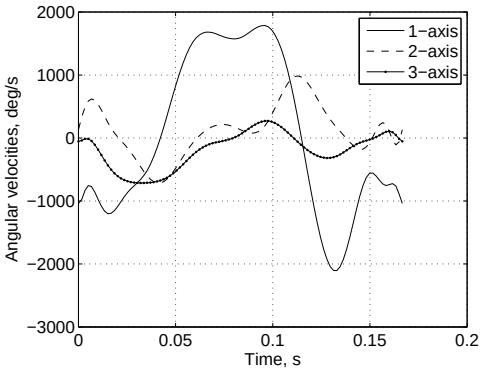

(a) Angular velocities

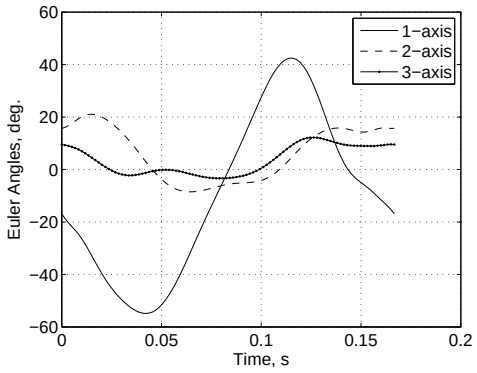

(b) Euler angle orientation

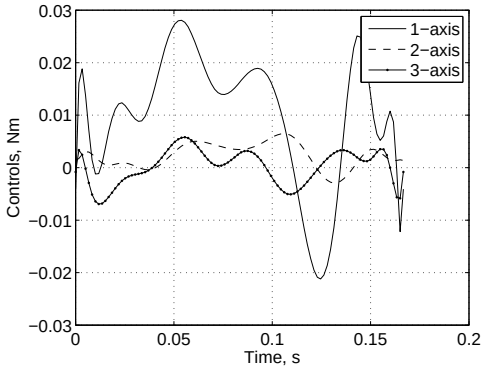

(c) Controls

Fig. 12. Case 2. Angular velocity, orientation and control time histories.

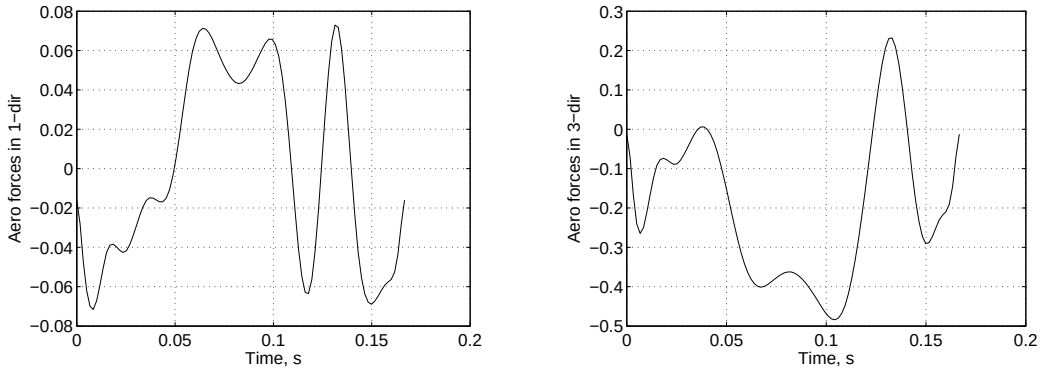

(a) Total aerodynamic force in inertial 1-direction

(b) Total aerodynamic force in inertial 3-direction

Fig. 13. Case 2. Total aerodynamic forces on the vehicle in the inertial frame.

3. Case 3

The wing stroke generated for Case 3 corresponds to a $\gamma_r = 0°$ and a $V_r = 6m/s$. It is shown here that the method can be used to design wing strokes that will maintain the vehicle at a near trim velocity other than $8m/s$. A velocity slower than the cruise velocity of the Barn Swallow is chosen because it falls closer to the minimum of the calculated power curve for the corresponding fixed wing vehicle. Fig. 14 shows the wing stroke for Case 3.

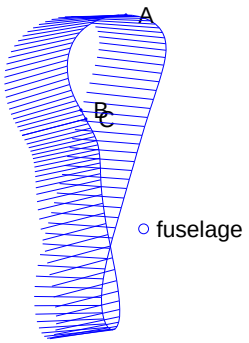

Fig. 14. Case 3. Wing stroke, inertial view from wing tip. This is the history of the wing mean geometric chord over the stroke period.

Figs. 15(a)-15(c) show the velocity and flight path angle of the vehicle and the angle of attack of the wings for Case 3. Notice the higher angles of attack. Figs. 16(a)-16(c) are the angular velocities, orientation and control histories for Case 3. Figs. 17(a) and 17(b) show the aerodynamic force histories for Case 3.

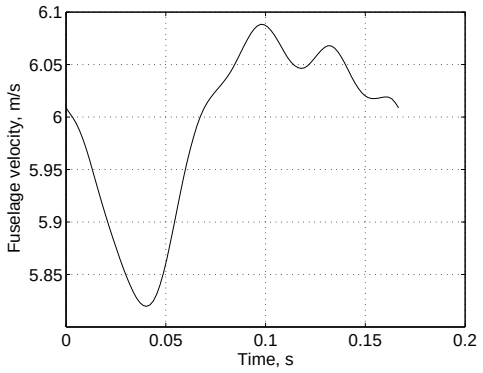

(a) Flight path velocity

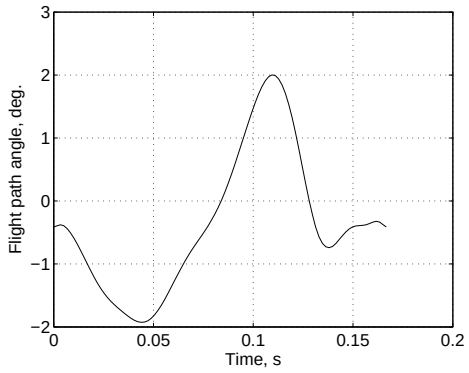

(b) Flight path angle

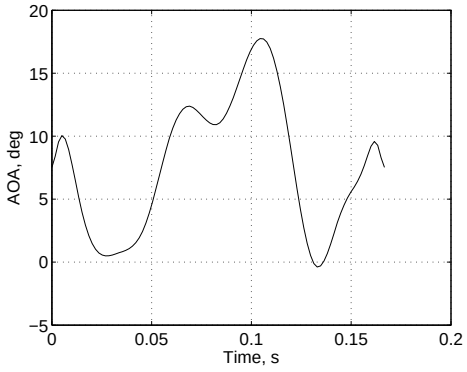

(c) Angle of attack

Fig. 15. Case 3. Velocity, flight path angle and effective angle of attack time histories.

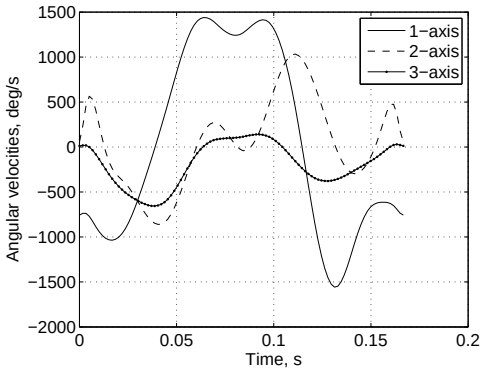

(a) Angular velocities

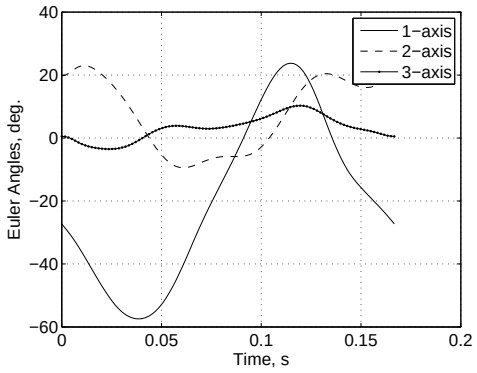

(b) Euler angle orientation

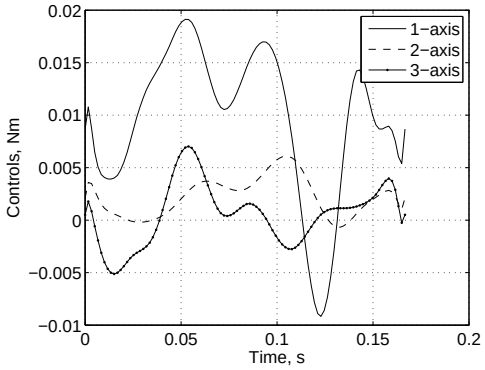

(c) Controls

Fig. 16. Case 3. Angular velocity, orientation and control time histories.

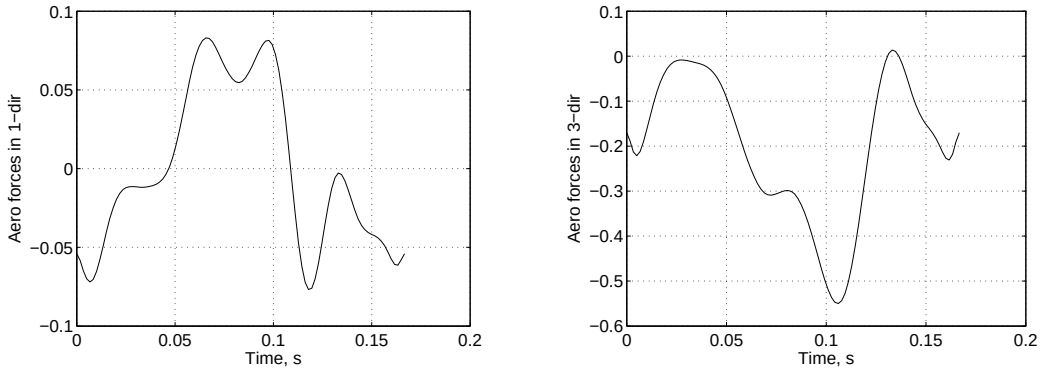

(a) Total aerodynamic force in inertial 1-direction

(b) Total aerodynamic force in inertial 3-direction

Fig. 17. Case 3. Total aerodynamic forces on the vehicle in the inertial frame.

4. Application of the optimized control

As a step taken to validate the optimization routine used to optimize the wing stroke of the flapping wing vehicle, the control obtained from the optimization that corresponds to the optimized state histories was applied in an open loop manner to the simulated system. Figs. 18, 19, 20 and 21 show the velocity, control, Euler angle and angular velocity histories for the application of the optimized control. In Figs. 18,20 and 21, the states begin to slowly diverge as the optimized control is applied. This divergence of the states from the optimized states occurs because the solution from the optimization comes from an approximation that lies on a subspace of the space that contains the actual optimal solution.

The simulation is run for 2 seconds, which is enough to see the divergence of the velocity, flight path angle, Fig. 18, and Euler angle, Fig. 20, states. The divergence is not as noticable in the angular velocities, Fig. 21, and the controls, Fig. 19 are the controls from the optimization. At the start of the simulation, the states follow very well because the control needed to maintain the states on the trajectory are very close to the reference controls. As the states begin to diverge, the control needed to bring the states back to the trajectory do not correspond to the optimized control histories.

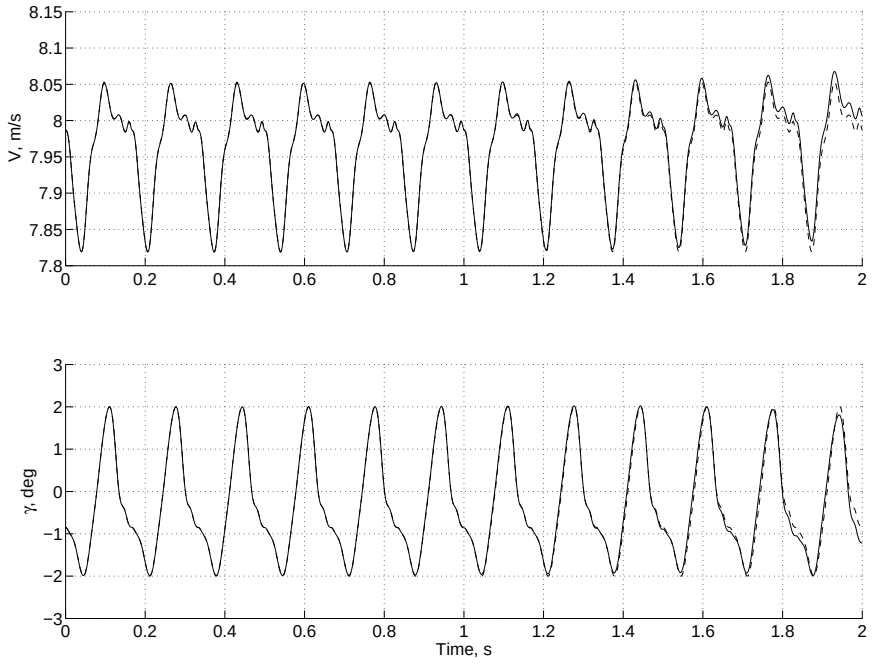

Fig. 18. Velocity and flight path angle histories for applying the control from the optimization. Control is repeatedly applied for 12 wing beats. Plots are for the example in Case 1.

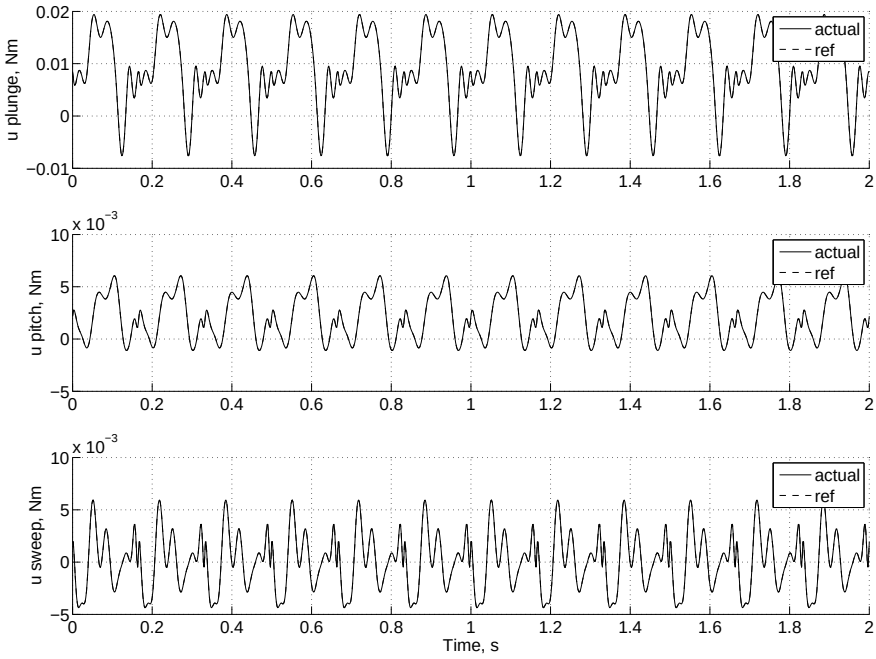

Fig. 19. Applied controls from optimization. Control is repeatedly applied for 12 wing beats. Plots are for the example in Case 1.

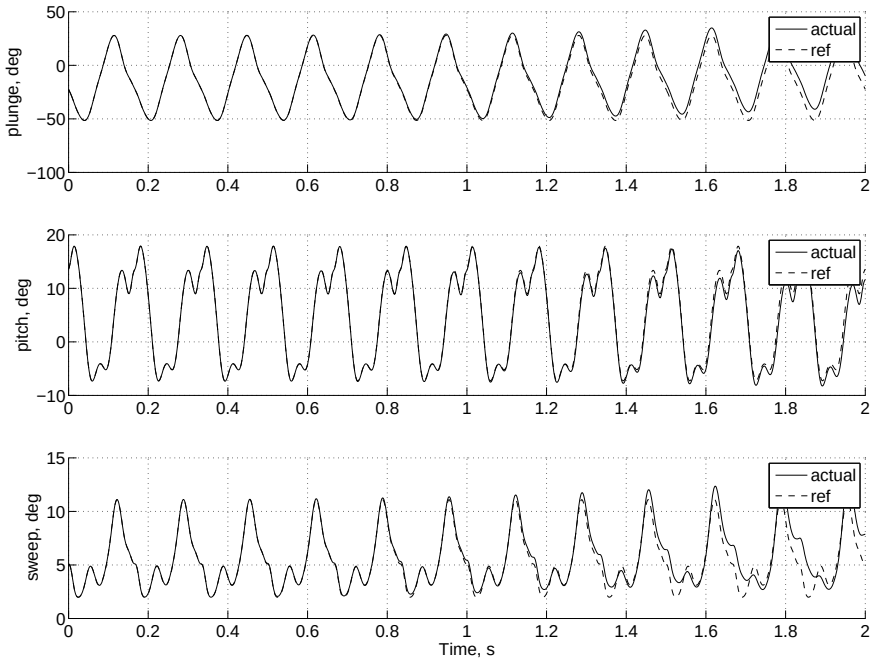

Fig. 20. Euler angle orientation time histories for applying the control from the optimization. Control is repeatedly applied for 12 wing beats. Plots are for the example in Case 1.

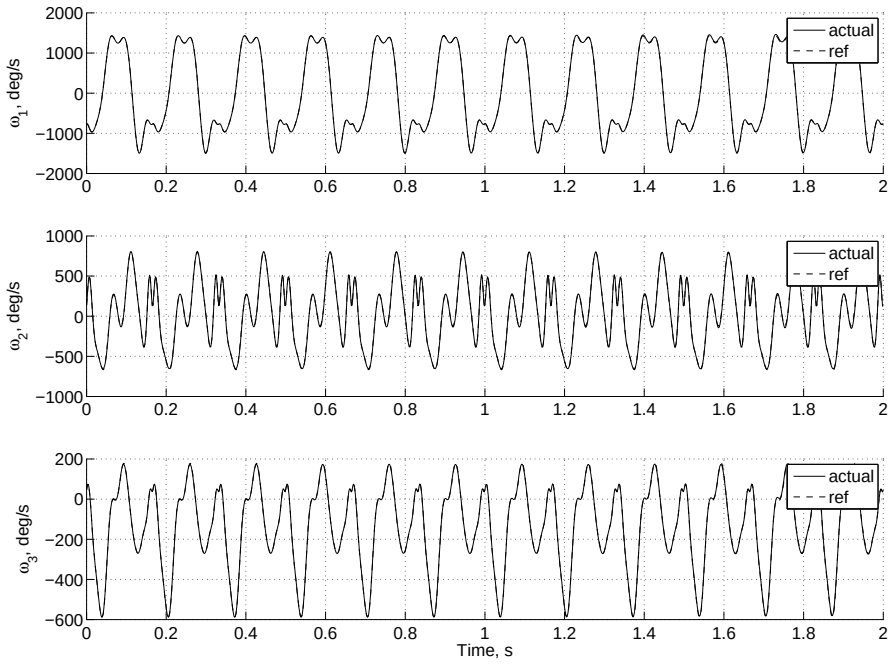

Fig. 21. Angular velocity time histories for applying the control from the optimization. Control is repeatedly applied for 12 wing beats. Plots are for the example in Case 1.

B. Linearization and gliding stability results

The eigenvalues of the linearized system from Chapter VII are presented here. The eigenvalues of the system linearized about various trim configurations are examined. Three trim configurations are used here. For all, the plunge angle is fixed and the sweep angle is varied to obtain a static configuration. The first is with a plunge angle of $0°$, the second and third cases are with the plunge angle fixed at $-10°$ and $-30°$ respectively. With the plunge angle fixed, the corresponding sweep and pitch angles are solved for using the optimization technique from Chapter VII. These configurations are detailed in Table III. These configurations were chosen to demonstrate the change in the sweep angle corresponding to a trimmed configuration for various positive dihedral angles. It is seen that when the dihedral increases, the trim sweep angle of the wings is farther backward, this is because the moment from the drag of the wings is greater. With the larger moment arm, the moment created from the drag of the wings is better able to counteract the opposite moment from the lift force. Table IV contains the resulting flight path angles, angles of attack and lift to drag ratios for each of the gliding configurations. The eigenvalues of the system tell the local stability of the system near the trim condition. Eigenvalues and time constants for the three configurations are presented in Table V. Recall that the trim configuration is determined by fixing the velocity magnitude and either the plunge or sweep angle of the wings and solving an optimization problem that minimizes the total pitching moment on the vehicle while satisfying the constraints in Eqs. 7.16 and 7.17. The values of the flight path angle, sweep or plunge angle, pitch angle and the three control moments result from the solution.

Table III. Gliding configurations

Orientation angle	**Case 1**	**Case 2**	**Case 3**
$plunge, \theta(1)$, °	0	-10	-30
$pitch, \theta(2)$, °	-2	-4.488	-8.509
$sweep, \theta(3)$, °	-14.849	-14.292	-12.272

Table IV. Gliding α's and γ's

	Case 1	**Case 2**	**Case 3**
V, m/s	8	8	8
γ, °	-5.719	-5.81	-6.546
α, °	3.916	4	4.613
L/D	9.985	9.828	8.715

Table V. Eigenvalues and time constants

Associated state			
Eigenvalues	**Case 1**	**Case 2**	**Case 3**
V	-0.07	-0.071	-0.079
γ	-5.019	-4.719	-3.380
Time constant, s			
V	14.279	14.085	12.698
γ	0.2	0.212	0.296

Fig. 22 shows the velocity and flight path angle time histories in gliding flight for Case 2. The velocity states behave in an open loop manner while the Euler angle orientations of the wings do not change with time, they are fixed at values corresponding to the gliding trim of the vehicle, the angular velocities of the wings are zero for all time. The simulation in Fig. 22 demonstrates the slow convergence of the flight path velocity and the relatively fast convergence of the flight path angle mode. The slow convergence of the flight path velocity mode is consistent with conventional aircraft and is associated with the long period Phugoid mode [14].

Because the wing orientation is inertially fixed, the change in angle of attack is exclusively a function of the flight path angle. For conventional aircraft, the mode associated with changes in angle of attack is the Short Period mode referred to as such because it is generally a high frequency oscillatory mode which also has very high damping. The Short Period mode is generally associated with a change in angle of attack and pitch attitude, [14], for this case the angle of attack and flight path angle are the participants, App. A. This fast convergence of the flight path angle can be seen in Fig. 22.

In Chapter VII a simplification was made that allowed the extraction of the stability characteristics associated with the velocity and flight path angle states. This simplification involved reformulating the system in terms of two states, the two inertial velocities, and three controls, the orientation of the wings. Recall that this simplification assumes that the orientations of the wings can be controlled instantaneously. For gliding flight, this is reasonable as small perturbations about the equilibrium are considered. Eqs. 7.37, 7.35 and 7.36 are the the linear system and

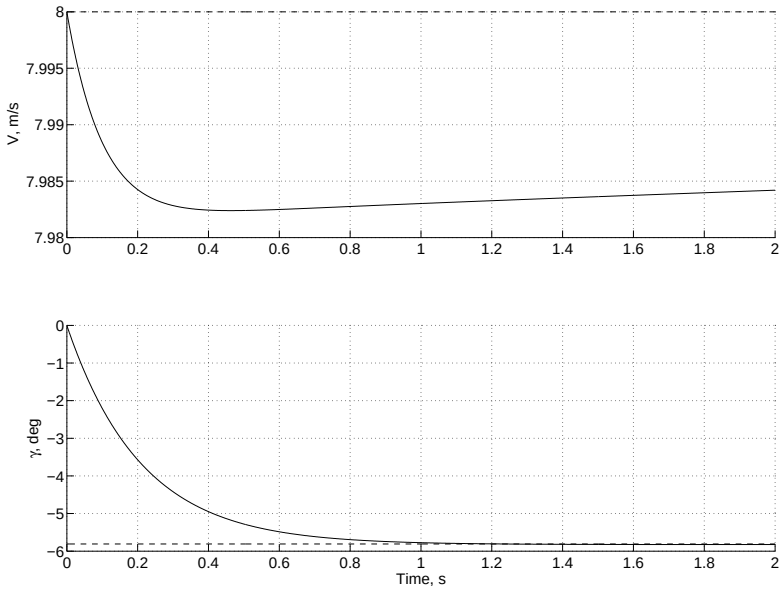

Fig. 22. V and γ time histories for wing orientation fixed in gliding position. Initial $\gamma = 0$. Trim $\gamma = -5.81°$

the associated states and controls for the system considered here. For Case 2 above, the linearized system matrices, $[A]$ and $[B]$ are

$$[A] = \begin{bmatrix} -0.0538 & 0.4623 \\ -0.1738 & -4.737 \end{bmatrix}, \tag{9.1}$$

$$[B] = \begin{bmatrix} 4.926 & -17.211 & 3.588 \\ 4.745 & -37.745 & 7.593 \end{bmatrix}. \tag{9.2}$$

The controllability matrix for the two state system in Eq. 7.37 is

$$[C_n] = [B, AB] \tag{9.3}$$

$$= 10^2 \begin{bmatrix} 0.0493 & -0.1721 & 0.0359 & 0.0193 & -0.1652 & 0.0332 \\ 0.0474 & -0.3775 & 0.0759 & -0.2333 & 1.8178 & -0.3659 \end{bmatrix}. \tag{9.4}$$

This controllability matrix is full rank, as such, the system in Eq. 7.37 is controllable.

C. Trajectory tracking results

Results are presented here from tracking simulations of the example flapping wing vehicle. Three cases are presented here. The first case is with no initial tracking error, the initial state of the system lies on the trajectory being tracked which is a flapping trajectory. The second begins in a gliding configuration and transitions to a flapping trajectory. The third case begins with the states lying on the flapping trajectory and transitions to gliding flight. Gliding and flapping are used because they represent two important means of longitudinal flight. The gliding regime represents the rest configuration of the vehicle, or configuration in which the controls due no work because the angular velocities are zero. In this configuration, the vehicle can relinquish altitude and maintain velocity. If a flapping wing vehicle is to perform missions of various types, it would be wise to consider using gliding flight wherever possible in mission design. The flapping regime represents powered flight and is the only means by which the vehicle can maintain a flight path angle greater than that corresponding to the highest gliding flight path angle. Considering these two basic flight conditions, one is naturally led to the question of, how does the vehicle behave when transitioning from gliding to flapping flight and from flapping to gliding flight? The trajectory tracking results presented here will focus largely on an analysis of this question.

1. No initial tracking error

Figs. 23 and 24 present the flight path velocity, flight path angle and control time histories for a flapping wing stroke corresponding to a $V_r = 8\text{m/s}$ and a $\gamma_r = 0°$.

Notice that the velocity and flight path angle stay very near the the reference velocity and flight path angle. The curves for the controls, Fig. 24, also kiss the reference curves. Figs. 25 and 26 are the plots of the Euler angle and angular velocity histories of the wings as they track the reference. It is evident here that the states track the reference very well.

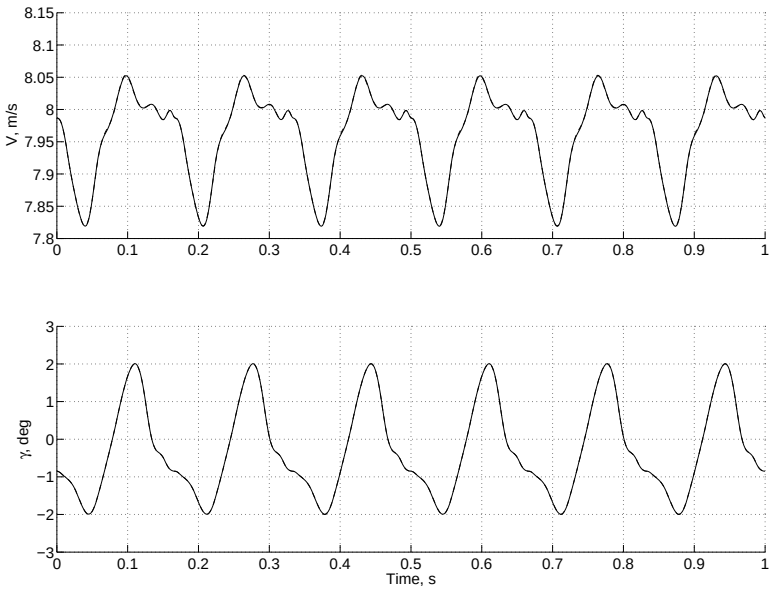

Fig. 23. Velocity and flight path angle histories for tracking a flapping stroke with no initial condition error.

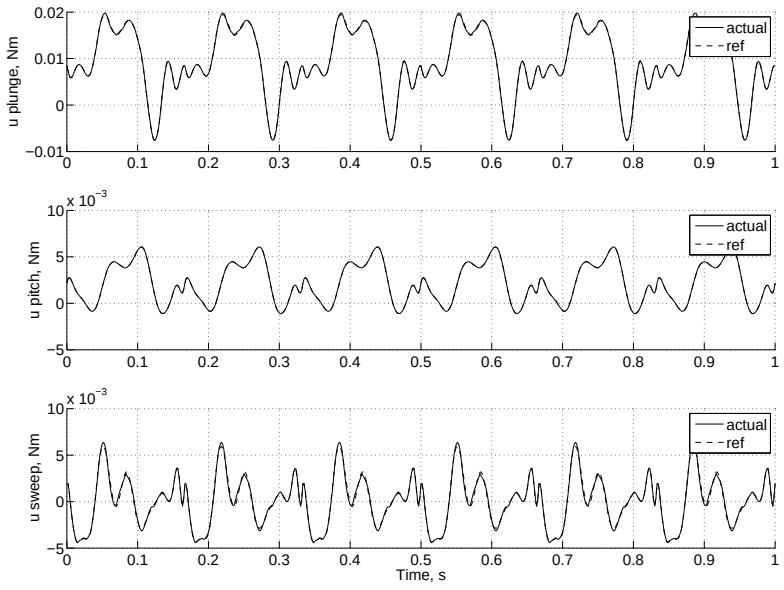

Fig. 24. Control time histories for tracking a flapping stroke with no initial error.

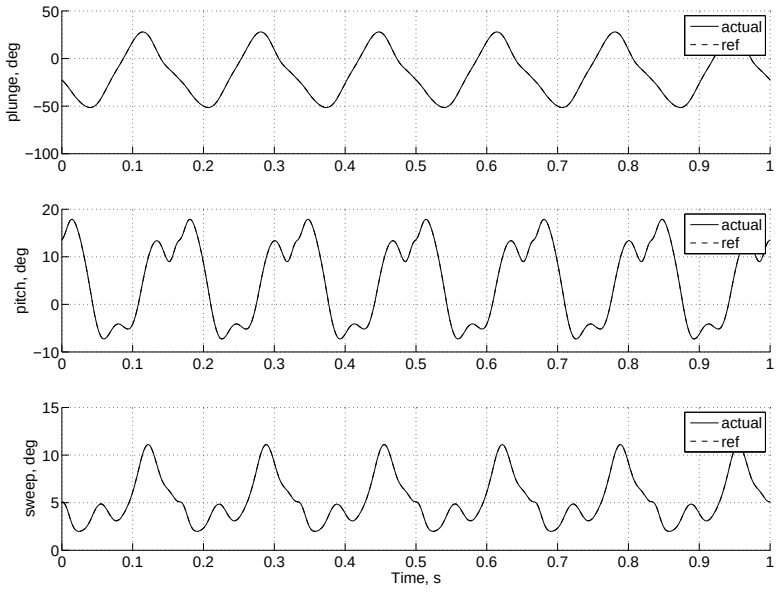

Fig. 25. Euler angle orientation time histories for tracking a flapping stroke with no initial error.

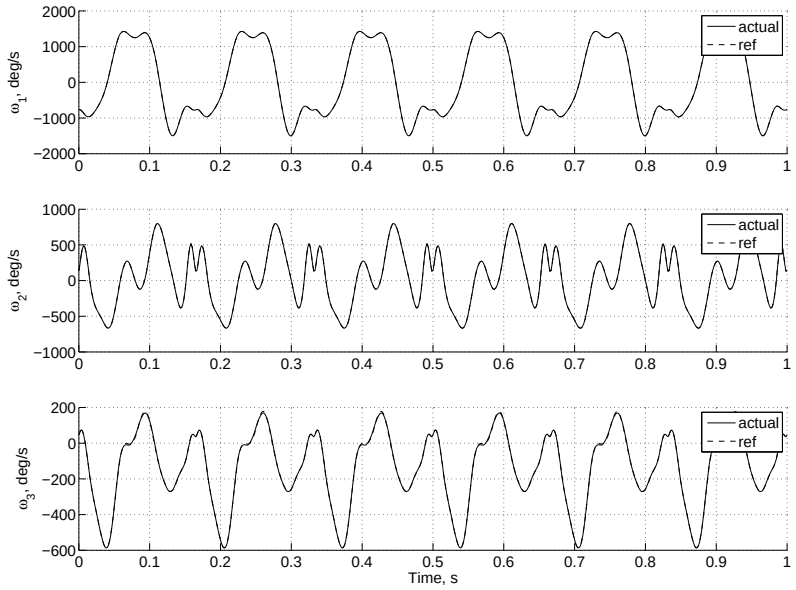

Fig. 26. Angular velocity time histories for tracking a flapping stroke with no initial error.

2. Initial gliding to flapping

Figs. 27 and 28 show the velocity and flight path angle histories where the initial conditions correspond to a gliding condition, but the wings are made to track a flapping stroke that corresponds to a $V_r = 8m/s$ and a $\gamma_r = 0°$. The vehicle begins with a negative flight path angle that becomes more negative as the stroke proceeds and rises shortly into the stroke. At the same time the velocity dips slightly, but rises fairly quickly and gradually begins to settle down to the reference value. Notice that the actual control inputs begin to catch up to the control inputs corresponding to the optimal wing stroke inside of two wing beats. The flight path angle begins to closely follow the curve for the given wing stroke fairly quickly, but the velocity takes much longer to reach the equilibrium. This is consistent with the results of Sec. B where it was seen that the flight path angle mode has a very short time constant and converges very quickly as compared to the flight path velocity mode that has a much longer time constant and slower convergence.

Figs. 29 and 30 are plots of the Euler angle and angular velocity time histories over one second. The fast convergence of these states is clear from the plots. The good performance of the controller is due to the canceling of the system dynamics by the controller.

Fig. 31 presents the velocity and flight path angle errors. Fig. 32 presents the Euler angle error kinematics and the associated rates. The convergence behaviors can be seen more clearly from the velocity and flight path angle error plots. The velocity error approaches zero very slowly while the flight path angle error decreases very quickly, but still exhibits a longer settling time. The Euler angle errors and their

rates demonstrate fast convergence and can be seen to follow the reference closely after about 1.5 wing beats. Notice the small jitters in the plot of Euler angle error rate, this phenomenon is not completely understood. It beats at a frequency close to the wing beat frequency and tends to be about three orders of magnitude smaller than the reference signal and is noticeable when the controller reaches steady state tracking.

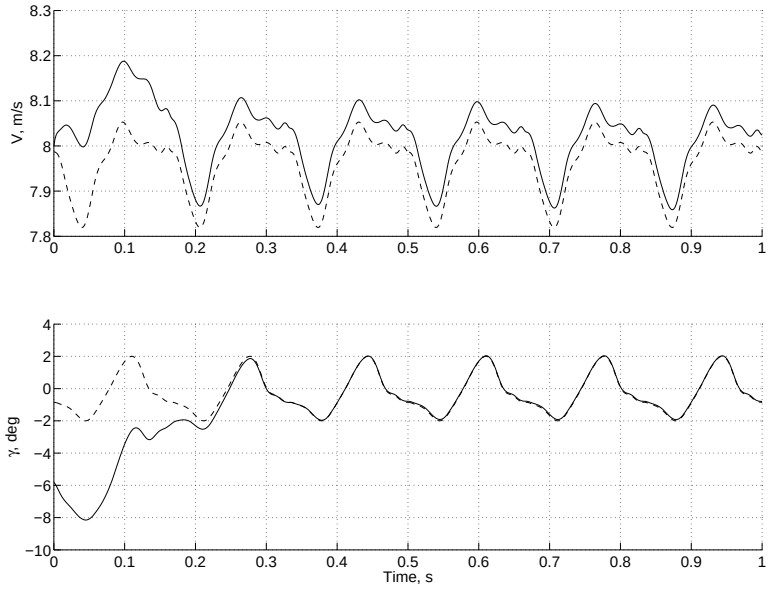

Fig. 27. Velocity and flight path angle time histories for tracking a flapping stroke stroke starting at an initial gliding configuration.

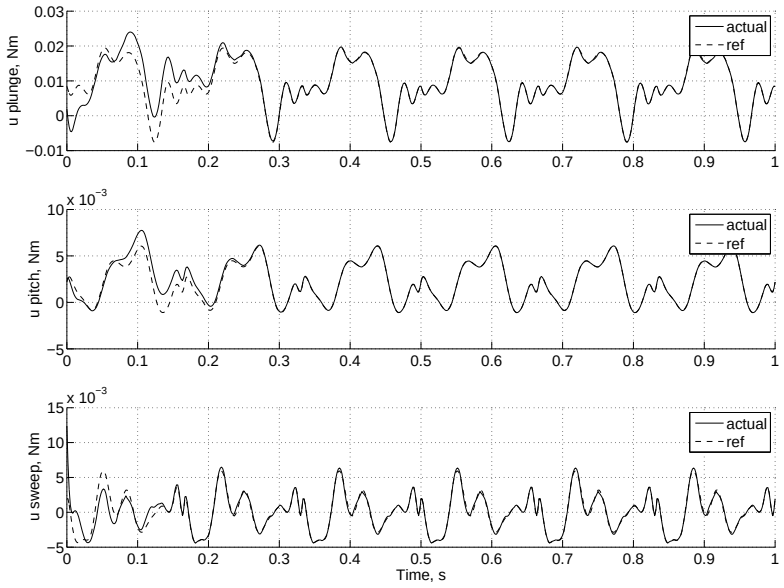

Fig. 28. Control time histories for tracking a flapping stroke starting at an initial gliding configuration.

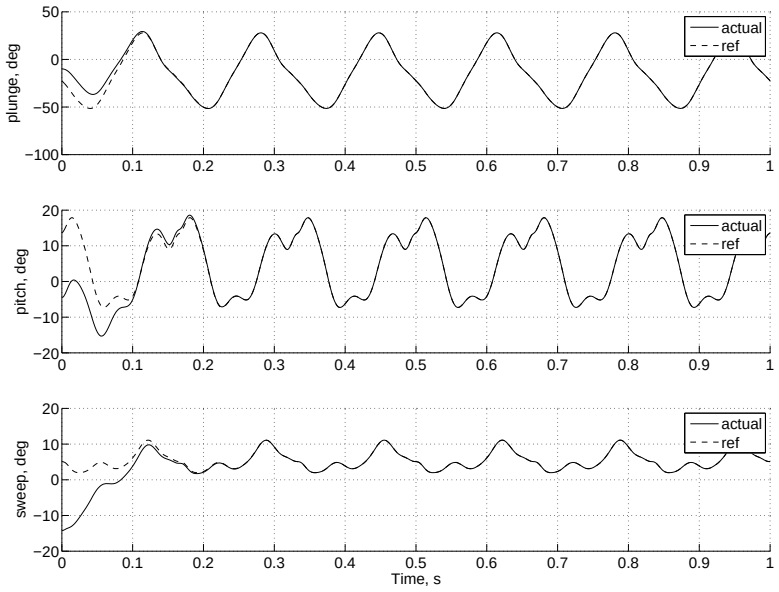

Fig. 29. Euler angle orientation time histories for tracking a flapping stroke starting at an initial gliding configuration.

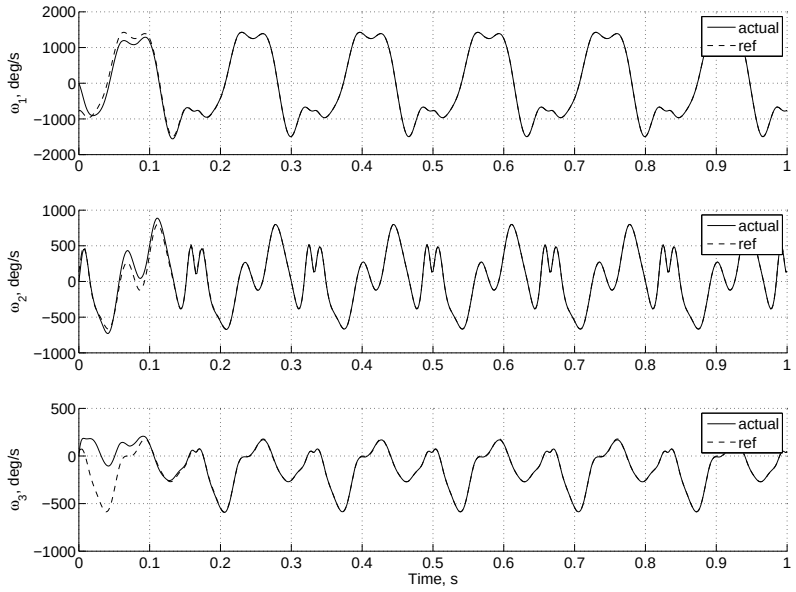

Fig. 30. Angular velocity time histories for tracking a flapping stroke starting at an initial gliding configuration.

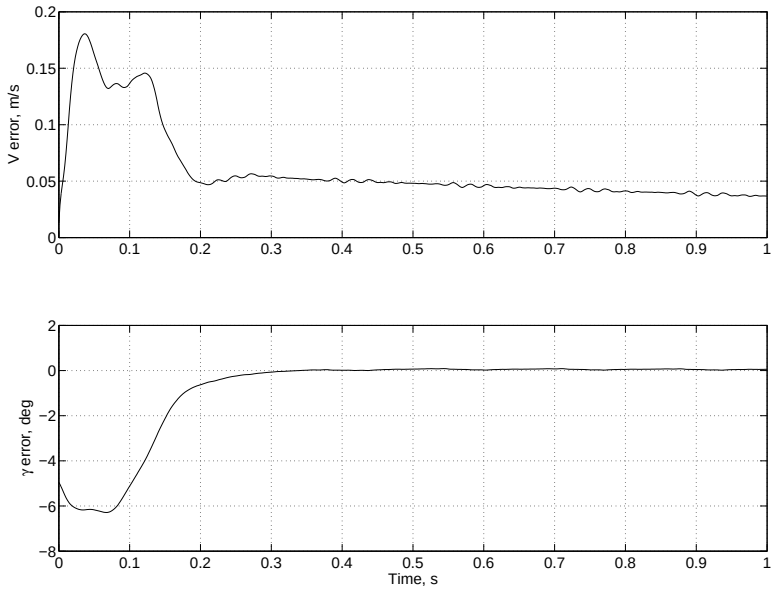

Fig. 31. Velocity and flight path angle errors for tracking a flapping stroke starting at an initial gliding configuration.

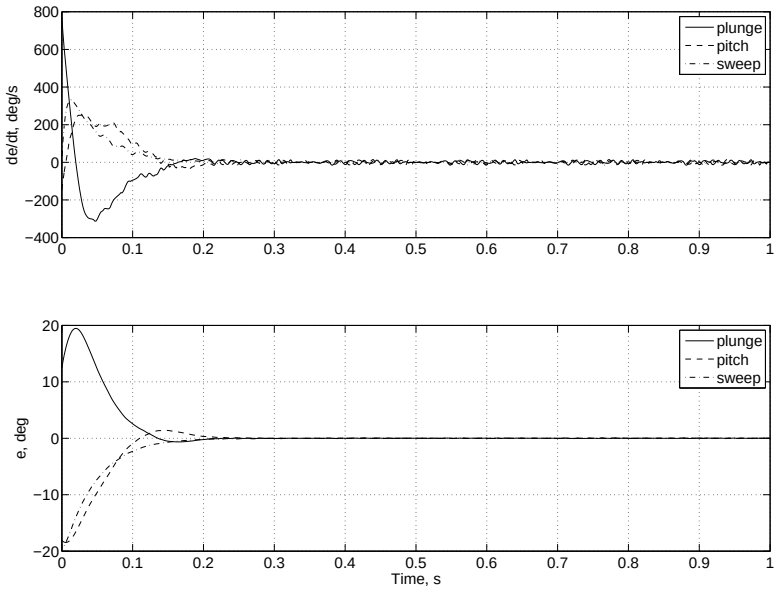

Fig. 32. Orientation error kinematics for tracking a flapping stroke starting at an initial gliding configuration.

3. Initial flapping to gliding

Figs. 33 and 34 show the behavior of the velocity, flight path angle and control inputs for a simulation that begins with the wings in a flapping configuration but the system is made to track a gliding configuration. In Fig. 33, the velocity immediately decreases away from the equilibrium as the flight path angle increases, also away from its equilibrium due to the initial configuration of the system. Again, the velocity mode shows slow convergence and the flight path angle mode converges quickly. Notice the slight offset of the flight path angle from the reference toward the end of the simulation. This is likely due to the relative values of the controller gains.

Figs. 35 and 36 demonstrate the velocity and flight path errors and the orientation error rates and orientation errors respectively. The Euler angles and angular velocities for the flapping configuration to gliding configuration case are seen in Figs. 37 and 38. Here, both sets of kinematics promptly converge to the equilibrium configuration with minimal overshoot in the Euler angles.

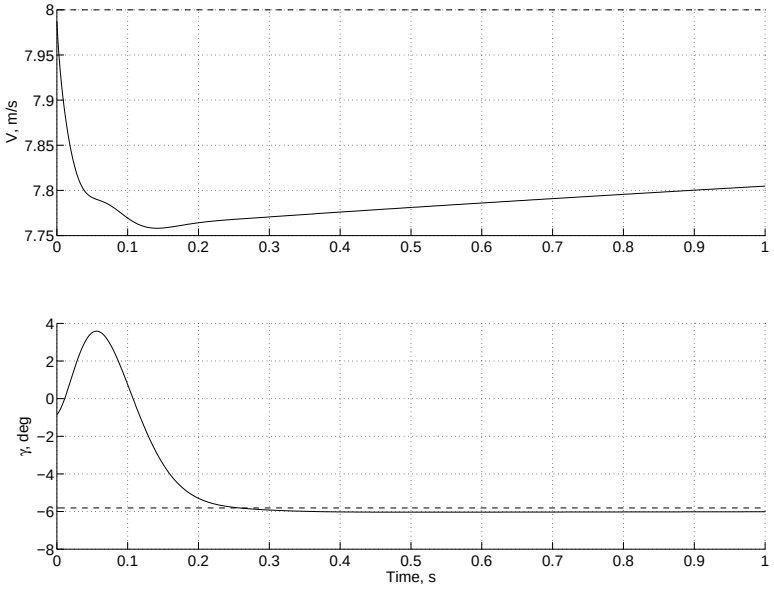

Fig. 33. Velocity and flight path angle time histories for tracking a gliding configuration starting at an initial flapping orientation.

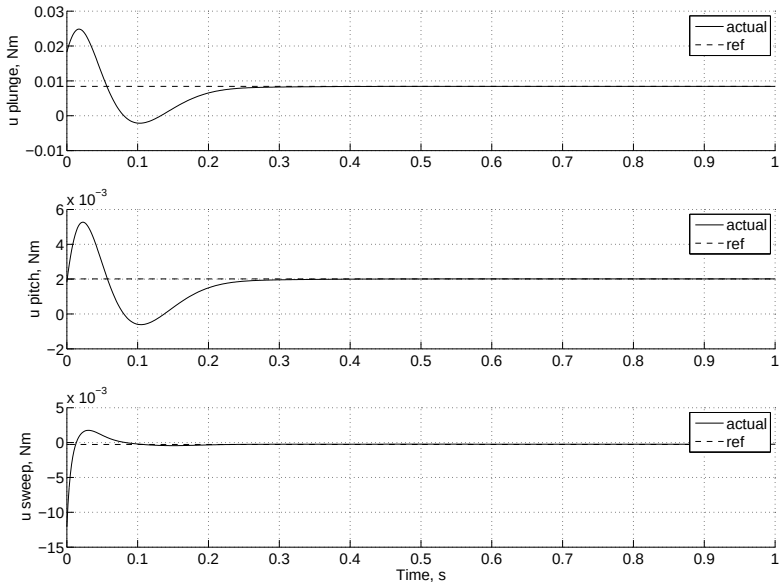

Fig. 34. Control time histories for tracking a gliding configuration starting at an initial flapping orientation.

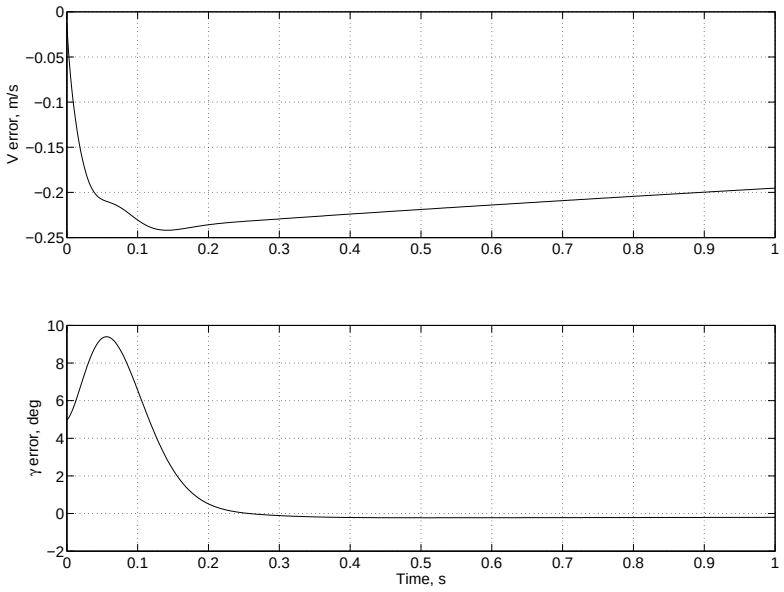

Fig. 35. Velocity and flight path angle errors for tracking a gliding configuration starting at an initial flapping orientation.

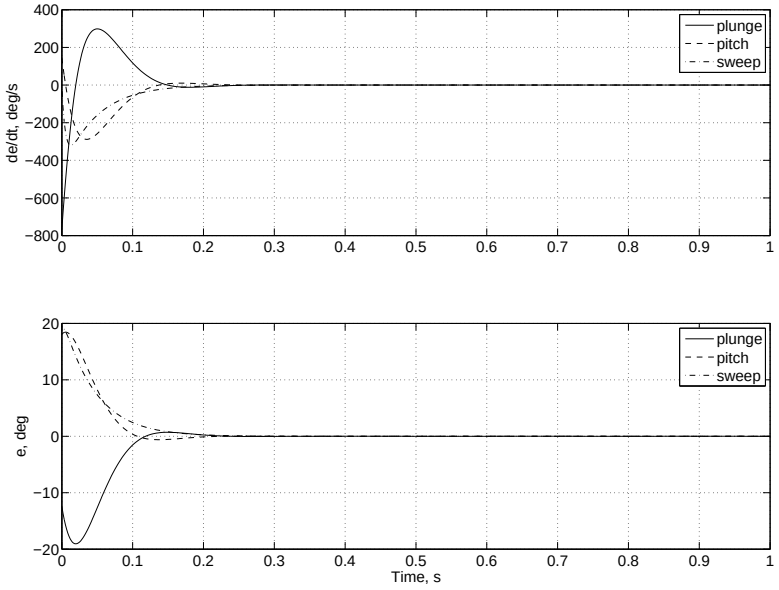

Fig. 36. Orientation error kinematics for tracking a gliding configuration starting at an initial flapping orientation.

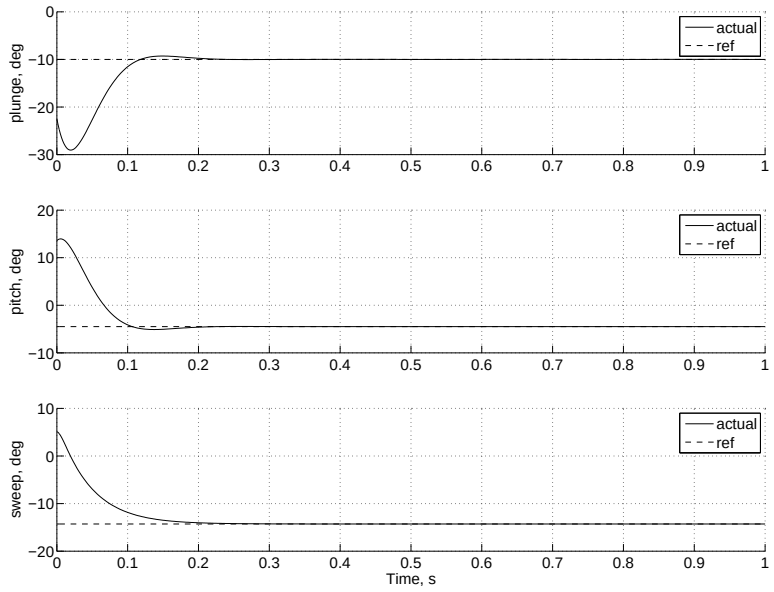

Fig. 37. Euler angle orientation time histories for tracking a gliding configuration starting at an initial flapping orientation.

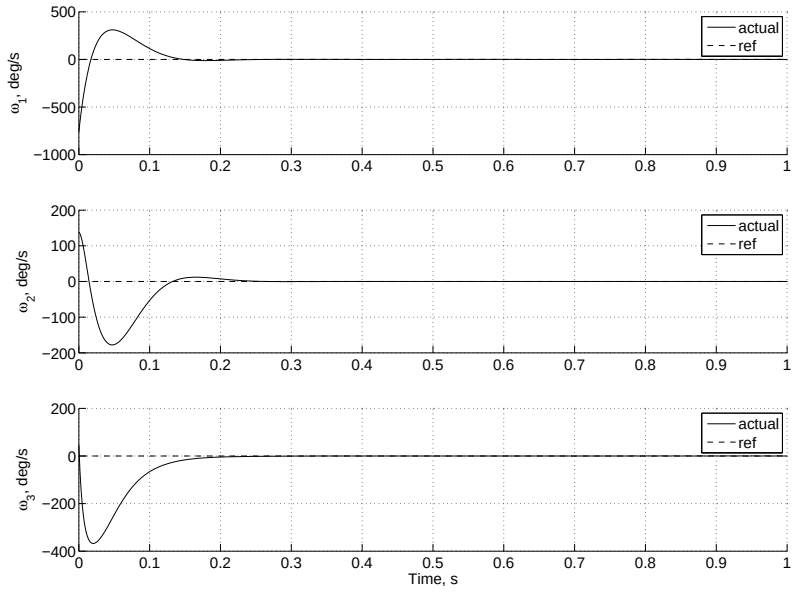

Fig. 38. Angular velocity time histories for tracking a gliding configuration starting at an initial flapping orientation.

D. Translational stability in flapping flight

Tracking results from simulations with initial perturbations in velocity and flight path angle are discussed here. The velocity and flight path angle errors do not influence the controller, because of this, these states are only guaranteed to satisfy the equations of motion and because the system is nonlinear, these states could potentially settle at values that satisfy the equations of motion but do not lie on the reference trajectory. The purpose of this section is to get an idea of how these states behave when they are perturbed and tracking states are not. For example, if the vehicle is subjected to a wind gust.

1. Velocity perturbation

Fig. 39 shows the response of the velocity and flight path angle of the vehicle when the velocity is initialized at 10% above the starting velocity for a flapping wing stroke of $V_r = 8m/s$ and $\gamma_r = 0°$. The simulation is run for six seconds to better demonstrate the behavior. The velocity and flight path angle converge toward the trajectory and seek the nearest equilibrium, in this case, the one corresponding to the wing stroke being used.

This trim seeking behavior can be seen better in Fig. 40 where the velocity and flight path angle errors relative to the reference are plotted. In Fig. 40, the convergent behavior of the velocity is clear. The flight path angle error however shows very different behavior from the analysis in Sec. B. Here, the flight path angle error is seen to oscillate, where as for gliding flight, the error converged monotonically. Notice that the flight path angle error does not converge noticeably quicker as compared to

the velocity error for this case.

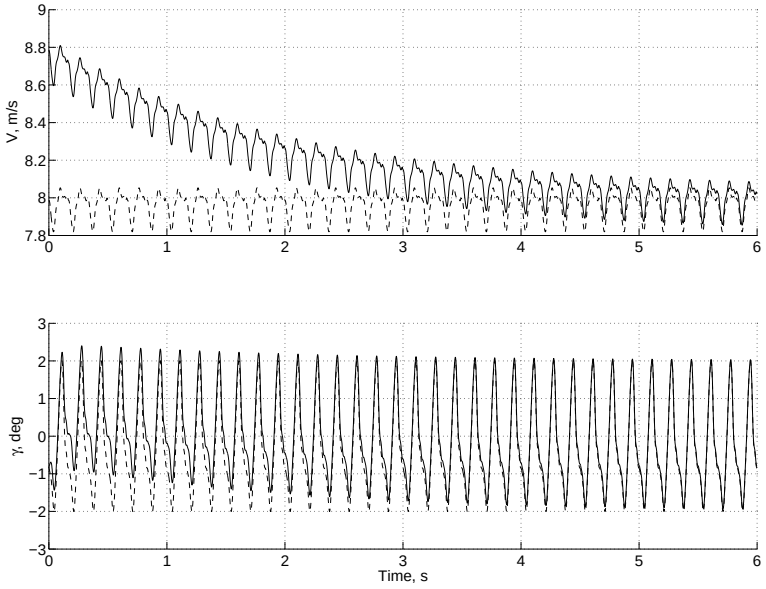

Fig. 39. Velocity and flight path angle histories for tracking a flapping stroke with initial velocity error

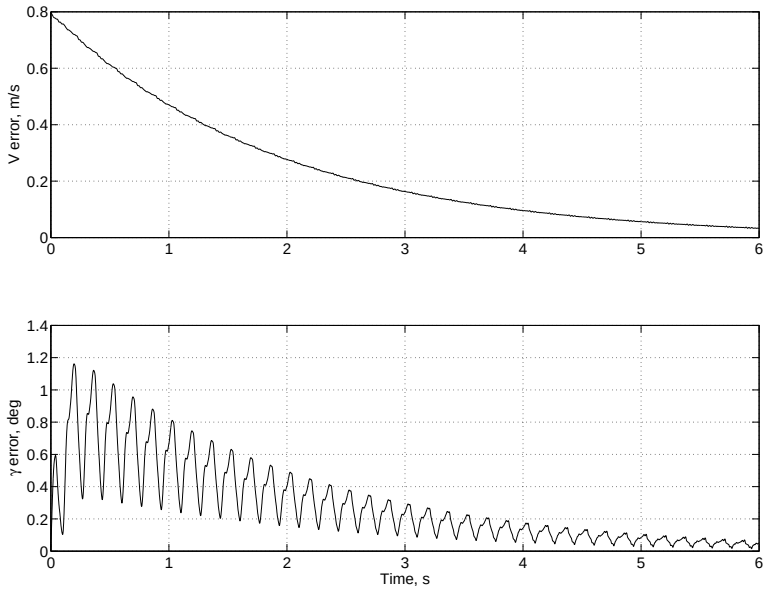

Fig. 40. Velocity and flight path angle error histories for tracking a flapping stroke with initial velocity error

2. Flight path angle perturbation

The velocity and flight path angle responses to a perturbation in the system flight path angle are presented in Fig. 41 for a flapping wing stroke of $V_r = 8m/s$ and $\gamma_r = 0°$. The behavior of the system in this case is quite different from the case of initial velocity perturbation. Here the flight path angle quickly returns to the equilibrium where the velocity is slightly perturbed with the change in flight path angle and slowly resumes following the reference values.

Fig. 42 demonstrates the rapid return of the flight path angle to the equilibrium in a less ambiguous way. This shows a convergent behavior very similar to that in Sec. B. The jitters once again appear in the errors and are similar to those found in Fig. 32.

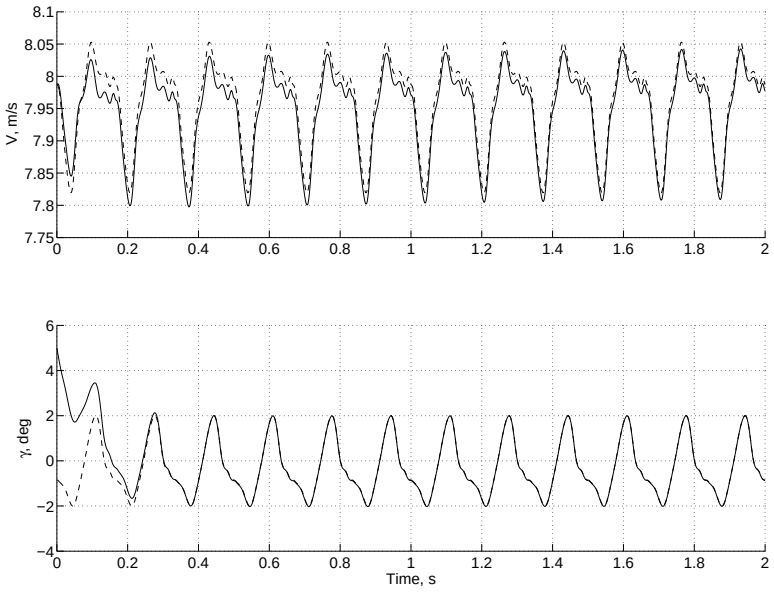

Fig. 41. Velocity and flight path angle histories for tracking a flapping stroke with initial flight path angle error

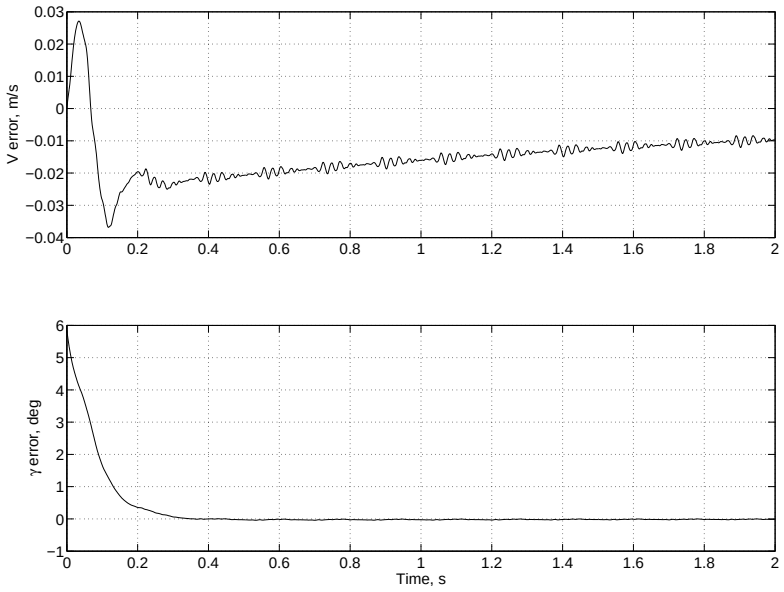

Fig. 42. Velocity and flight path angle error histories for tracking a flapping stroke with initial flight path angle error

E. Discussion of assumptions

This work contains many assumptions intended to bring tractability to the problem. Assumptions were made in all areas including the vehicle dynamics, aerodynamics, optimization and tracking control. These assumptions allowed for the effective study of the flapping wing problem without becoming lost in the many directions that this work could follow. The purpose of this research was to gain an insight into how one can design a wing stroke for a given flapping wing vehicle that when implemented will achieve a useful result for the vehicle as defined by the cost function, Chapter VI.

Major assumptions associated with the dynamic model of the vehicle include the rigid body assumption of the wing dynamics and the point mass fuselage assumption. In reality, flapping wing vehicles have both fuselage rotational dynamics and flexible wing dynamics. Because of the point mass fuselage assumption, the fuselage of the vehicle is not able to offer any kind of stabilizing effect that might otherwise be present. The flexibility in the wings of aircraft effect the angle of attack of the wings and whether the deformation of the wings is passive or actively controlled, this inherent flexibility can have significant influence on the stability of the system.

The fuselage of the vehicle was assumed to have no aerodynamic effects and it was assumed that the aerodynamics of each of the wings was independent. In reality, the fuselage of the vehicle would have significant aerodynamic contribution. The angle of attack of the vehicle fuselage could be controlled to achieve useful maneuvering characteristics for the vehicle such as velocity and flight path angle tracking.

The aerodynamic model used here is one of the simplest aerodynamic models available. This aerodynamic model does not incorporate the effects of higher reduced frequencies, viscosity or flow separation. In reality, all such effects influence a flapping wing vehicle the size of a bird or an insect. As seen in Table II, the reduced frequencies are within the range where the phase difference between the motion of the wings and the aerodynamic loads becomes significant. Small flapping wing vehicles fly in a regime of low Reynolds numbers, order of $10,000$, where quasi-steady assumptions break down. Only cruise flight for a fairly large flapping wing vehicle was considered here. In flight conditions such as hovering or other high angle of attack transient maneuvers, separation can occur, this is likely to have significant effect on the aerodynamics of the vehicle, but high angle of attack maneuvers and separation are not considered here.

CHAPTER X

CONCLUSIONS

This thesis has presented a method for designing a wing stroke for a flapping wing vehicle. A vehicle model was chosen so as to retain the useful substance of the flapping problem and still allow for wing and fuselage dynamics. Because longitudinal flight was the primary interest of this thesis, a symmetry constraint was imposed to ensure that the wings moved in a symmetric manner. Euler angle kinematics were used to describe the orientation of the wings relative to an inertial frame. The vehicle dynamics were described by five equations of motion, two for the translational velocity rate of the vehicle fuselage and three for the angular velocity rate of the wings. Because the fuselage was modeled as a point mass, there were no associated aerodynamic effects, the only aerodynamic forces were due to the wings of the vehicle. These aerodynamics were characterized by lift and drag forces on the wings that were functions of the instantaneous total angle of attack of the wings [14].

The purpose of this research has been to show that a flapping wing stroke for a vehicle that produces thrust by flapping its wings can be designed solving a well posed optimization problem that minimizes an appropriate cost function and has proper constraints. The cost function was a function of the parameters defining the desired maneuver, in this case the velocity and flight path angle of the vehicle. The optimal control problem was discretized using a Chebyshev Pseudospectral method, [28], and solved using the NLP solver FMINCON, [29]. The example chosen for demonstration of the method was a Barn Swallow. Gliding configurations of the

vehicle were solved for and the vehicle dynamics were numerically linearized about a specific gliding configuration [29].

A nonlinear controller was designed in Chapter VIII to track the wing strokes generated in Chapter VI. This controller was designed using a Dynamic Inversion methodology, [31], which ensured that the controller eliminated the nonlinear dynamics of the system and enforced a stable linear dynamics. The stability of the controller was proved using a Lyapunov method. The controller only guaranteed convergence of the orientation and the associated rates to the reference orientation and rates and did not guarantee convergence of the vehicle velocity states to the corresponding reference. Because the velocity states of the system must satisfy the dynamics of the system at the reference condition, the velocity states converge to a corresponding equilibrium; it was shown in simulation that this equilibrium corresponds to the reference trajectory.

An optimal control problem can be posed such that its solution results in a wing stroke that the wings of a flapping wing vehicle can track in order to achieve a desired maneuver. This formulation is modular and can accommodate other aerodynamic models and the dynamics of different vehicles. The gliding and flapping wing dynamics of the system that were demonstrated here show good agreement with known stability and control characteristics of conventional aircraft. The method presented in this thesis demonstrates a novel way to analyze the flapping wing problem from a total dynamical system point of view. This technique is able to account for the dynamics of the whole system and is built around achieving a useful result for the whole vehicle instead of maximizing the thrust or lift of the wings over the course of

a flapping stroke.

Through linearization about a number of trim configurations, it was seen that gliding flight is stable in many vehicle configurations. Different gliding configurations also correspond to different flight path angles for a given velocity and thus, offer a family of configurations that can be used to maneuver in gliding flight.

Nonlinear tracking control laws can be used to track these wing strokes and accomplish the desired maneuver. However, these control laws require precise knowledge of the system dynamics and aerodynamics which are not generally known in practice. This control law does help demonstrate the open loop stability of the velocity and flight path angle states when perturbed from the equilibrium corresponding to the particular wing stroke. The tracking law used helps demonstrate the stability of the system in transition from gliding to flapping flight as well as flapping to gliding flight. The control magnitudes also remain fairly close to those from the optimization values for the cases with initial state error.

It has been seen that the wings of a flapping wing vehicle generate lift and drag in much the same way that a fixed wing aircraft does. However, the wings of a flapping wing vehicle also must generate thrust to propel the vehicle forward and balance the drag force in trimmed flight. What is interesting is that the mechanism that produces the drag that apposes the vehicle translation is the same mechanism that generates the thrust to propel the vehicle forward. This is not seen in fixed wing flight.

There are many paths that the future of this work could follow. One of the more obvious paths being the extension of the aerodynamic model to quantify the

unsteady effects of the wing aerodynamics. For example, a vortex panel method is a common way to model the aerodynamics of flapping wings,[10, 7, 4], because it allows for the inclusion of wing tip effects as well as accounting for the influence of the vehicle wake. Neither of which are accounted for in the above formulation. Because the leading edge vortex that forms on the wing is known to be an important mechanism of lift production, [1, 11, 12, 13, 9], it would be appropriate to use a vortex panel method in the aerodynamic model so as to capture the interaction between the vehicle dynamics and this leading edge vortex.

Another path would be to include the vehicle dynamics and aerodynamics of the fuselage of the vehicle. The fuselages of most flapping wing vehicles found in nature are large and heavy as compared to the wings of the vehicle, because of this, the associated rotational dynamics and aerodynamics of the fuselage will have significant influence on the dynamics of the system. Another natural extension to this work would be to include lateral directional motion in the formulation. The cost function would be changed accordingly to ensure the wing stroke resulted in a desired heading angle as well as flight path angle; however, the dynamics of this system become much more complicated.

REFERENCES

[1] W. Shyy and H. Liu, "Flapping wings and aerodynamic lift: The role of leading-edge vortices," *AIAA Journal*, vol. 45, pp. 2817–2819, December 2007.

[2] S. D. Ross, "Optimal flapping strokes for self-propulsion in a perfect fluid," in *American Control Conference*, Minneapolis, MN, June 2006, pp. 4118–4122.

[3] M. Kaya and I. H. Tuncer, "Nonsinusoidal path optimization of a flapping airfoil," *AIAA Journal*, vol. 45, pp. 2075–2082, August 2007.

[4] K. C. Hall, S. A. Pignott, and S. R. Hall, "Power requirements for large-amplitude flapping flight," *Journal of Aircraft*, vol. 35, pp. 352–361, May-June 1998.

[5] R. C. Michelson and M. A. Naqvi, "Beyond biologically-inspired insect flight," in *von Karman Institute for Fluid Dynamics Lecture Series*, Brussels, Belgium, November 2003, pp. 1–19.

[6] T. Liu, K. Kuykendoll, and S. Jones, "Avian wing geometry and kinematics," *AIAA Journal*, vol. 44, pp. 954–963, May 2006.

[7] M. Lasek, J. Pietrucha, M. Zlocka, and K. Sibiliski, "Analogies between rotary and flapping wings from control theory point of view," in *AIAA Atmospheric Flight Mechanics Conference and Exhibit*, Montreal, Canada, August 2001, pp. 1–11.

[8] W. Shyy, M. Berg, and D. Ljungqvist, "Flapping and flexible wings for biological and micro air vehicles," *Progress in Aerospace Sciences*, vol. 35, pp. 455–505, 1999.

[9] H. Liu, C. P. Ellington, K. Kawachi, C. V. D. Berg, and A. P. Willmott, "A computational fluid dynamic study of hawkmoth hovering," *Journal of Experimental Biology*, vol. 201, pp. 461–477, January 1998.

[10] M. S. Vest and J. Katz, "Unsteady aerodynamic model of flapping wings," in *Aerospace Sciences Meeting and Exhibit*, San Diego, CA, January 1995, pp. 45–64.

[11] C. Van den Berg and C. P. Ellington, "The three-dimensional leading-edge vortex of a 'hovering' model hawkmoth," *Philosophical Transactions of the Royal Society of London, Series B: Biological Sciences*, vol. 352, pp. 329–340, March 1997.

[12] C. P. Ellington, C. V. D. Berg, A. P. Willmott, and A. R. Thomas, "Leading-edge vortices in insect flight," *Nature (London)*, vol. 384, pp. 626–630, December 1996.

[13] J. M. Birch and M. H. Dickinson, "Spanwise flow and the attachment of the leading-edge vortex on insect wings," *Nature (London)*, vol. 412, pp. 729–733, August 2001.

[14] J. Roskam, *Airplane Flight Dynamics and Automatic Flight Controls Part I*, Design, Analysis and Research Corporation, Lawrence, KS, 2003.

[15] D. Hodges and G. Pierce, *Introduction to Structural Dynamics and Aeroelasticity*, Cambridge University Press, New York, NY, 2002.

[16] B. Singh and I. Chopra, "Dynamics of insect-based flapping wings: Loads validation," in *AIAA/ASME/ASCE/AHS/ASC Structures, Structural Dynamics, and Materials Conference*, Newport, RI, May 2006, pp. 1–26.

[17] A. Jaroszewicza, K. Sibiliski, A. Sibilska, and A. Zyluk, "Biomimic sensors guided flight stability and control for flapping wings autonomous micro air vehicle (entomopter)," in *AIAA Aerospace Sciences Meeting and Exhibit*, Reno, NV, January 2007, pp. 1–34.

[18] X. L. Schenato and S. S. Deng, "Flight control system for a micromechanical flying insect: Architecture and implementation," in *International Conference on Robotics and Automation*, Seoul, Korea, May 2001, pp. 1641–1646.

[19] M. Lasek and K. Sibilski, "Modelling and simulation of flapping wing control for a micromechanical flying insect (entomopter)," in *AIAA Modeling and Simulation Technologies Conference and Exhibit*, Monterey, CA, August 2002, pp. 1–11.

[20] W. Dickson, A. Straw, C. Poelma, and M. Dickinson, "An integrative model of insect flight control," in *AIAA Aerospace Sciences Meeting and Exhibit*, Reno, NV, January 2006, pp. 1–19.

[21] R. C. Michelson and S. Reece, "Update on flapping wing micro air vehicle research," in *Bristol International RPV Conference*, Bristol, England, March

1998, pp. 1–11.

[22] V. A. Tucker, "Bird metabolism during flight: evaluation of a theory," *Journal of Experimental Biology*, vol. 58, pp. 689–709, October 1973.

[23] J. Fisher and S. R. Vadali, "Gyroless attitude control of multi-body satellites using an unscented Kalman filter," *Journal of Guidance, Control and Dynamics*, vol. 31, no. 1, pp. 245–262, 2008.

[24] J. Anderson, *Introduction to Flight*, McGraw-Hill, New York, NY, 2000.

[25] H. Shaub and J. Junkins, *Analytical Mechanics of Space Systems*, American Institute of Aeronautics and Astronautics, Inc., Reston, VA, 2003.

[26] J. E. Hurtado, *Kinematic and Kinetic Principles*, John E. Hurtado/Lulu, College Station, TX, 2007.

[27] J. Hurtado and J. Junkins, "Optimal near-minimum-time control," *Journal of Guidance, Control and Dynamics*, vol. 21, pp. 172–174, January-February 1998.

[28] F. Fahroo and M. Ross, "Direct trajectory optimization by a Chebyshev pseudospectral method," *Journal of Guidance, Control and Dynamics*, vol. 25, pp. 160–166, January-February 2002.

[29] A. Grace and Inc. MathWorks, *Optimization Toolbox for Use with MATLAB*, The MathWorks, Inc., Natick, MA, 1994.

[30] H. Tennekes, *The Simple Science of Flight*, The MIT Press, Cambridge, MA, 1992.

[31] K. Subbarao, M. Steinberg, and J. L. Junkins, "Structured adaptive model inversion applied to tracking aggresive aircraft maneuvers," in *Guidance, Navigation and Control Conference and Exhibit*, Montreal, Canada, August 2001, pp. 1–10.

[32] J. E. Slotine and W. Li, *Applied Nonlinear Control*, Prentice-Hall, Inc., Englewood Cliffs, NJ, 1991.

[33] R. Mukherjee and D. Chen, "Asymptotic stability theorem for autonomous systems," *Journal of Guidance, Control and Dynamics*, vol. 16, pp. 961–963, September-October 1993.

APPENDIX A

SOME BASICS OF FLIGHT MECHANICS

This discussion pertains to a standard longitudinal analysis of conventional fixed wing, powered aircraft.

Longitudinal motions are the up and down, forwards and backwards, and pitching motions of the vehicle. Longitudinal maneuvering considers the vehicle to be translating parallel to a vertical plane and is only concerned with translational velocity components of the vehicle that lie in this vertical plane and the angular velocity component that is perpendicular to this plane, or pitch rate. Thus, there are three degrees of freedom for a longitudinally maneuvering, fixed-wing aircraft.

Lateral-directional motions are the side to side, rolling and yawing motions of the vehicle. Lateral-directional maneuvering considers the vehicle to be translating parallel to a horizontal plane and is concerned with the sideways velocity of the vehicle. The angular velocities considered in lateral-directional maneuvering are the roll and yaw rates, or the angular velocity about an axis pointing through the nose of the aircraft and the angular velocity about an axis pointing in the downward direction, perpendicular to the aircraft. This leaves three degrees of freedom for a lateral-directionally maneuvering, fixed-wing aircraft.

An aircraft has a total of six degrees of freedom. For small amplitude maneuvers, it is prudent to assume the decoupling of the longitudinal and lateral-directional

motions. This thesis only considers the longitudinal motion of a flapping wing system.

Trimmed flight for a conventional aircraft, is defined as

$$[\dot{\mathbf{V}}] = \mathbf{0}, \tag{A.1}$$

$$[\dot{\omega}] = \mathbf{0} \tag{A.2}$$

That is, the translational velocity and the angular velocity of the vehicle as expressed in a body fixed frame must be constant. For a conventional aircraft, this leaves three useful flight conditions. These flight conditions are 'Steady Rectilinear Flight', 'Steady Level Turn', and 'Steady Symmetrical Pull-up'. The first case is the flight condition applied in this research and is defined by and constant flight path velocity and a constant flight path angle and is a purely longitudinal flight condition. The second involves a constant altitude turn that forms a circular path and is purely lateral directional. The third is a vertical loop and forms a circle on the longitudinal plane, this is purely a longitudinal maneuver.

The Phugoid mode is an oscillatory flight mode that occurs at a near constant angle of attack. The Phugoid oscillation is primarily due to a *change in velocity*. The period of this mode can be on the order of 30 seconds for large aircraft and the amplitude can be several hundred meters in altitude. The eigenvalues associated with this mode tend to be relatively small and the associated damping is generally low, resulting in a very slow decay of the oscillation.

The Short Period mode is an oscillatory flight mode that occurs at a near constant velocity. The Short Period oscillation is due primarily to a change in *angle of attack*. The period of this mode is usually on the order of a few seconds. This mode demonstrates a quick pitching motion as apposed to the slower 'rollercoaster like' motion of the Phugoid mode. The Short Period eigenvalues often show comparatively high damping, thus, this mode decays fairly quickly.

APPENDIX B

NOMENCLATURE

$[T]$	Symmetry mapping between the rotational kinematics of wings 1 and 2
α_{eff}	Total angle of attack of wing
γ	Vehicle flight path angle
ω	Angular velocity vector
θ	Euler angle orientation of wing
$\mathbf{u}$	Wing control moment vector
$\mathbf{e}$	Euler angle orientation error
$\mathbf{V}$	Vehicle velocity in inertial frame
ρ	Air density
AR	Aspect ratio
C_D	Non-dimentional drag
C_L	Non-dimentional Lift

C_{D_0} Zero lift non-dimentional drag

C_{L_0} Zero angle of attack non-dimensional lift

C_{L_α} Non-dimentional lift curve slope

d_q Wing frame mgqc vector

d_c Wing frame CG vector

e Oswald efficiency factor

g Acceleration of gravity

I_c Principle axis inertias of wing

m Mass of vehicle

m_1 Mass of wing 1

m_2 Mass of wing 2

mgc Mean geometric chord

$mgqc$ Mean geometric quarter chord point

R Scaling of second order effect of lift on drag

S Single wing planform area

T Stroke period

V_L Lyapunov function

V_{fp} Velocity in stability axis system

VITA

Justin Patrick Jackson is the son of Kenneth Jackson and Kimiko Rife and was born in Columbia, South Carolina. After graduating from McNeil High School in Austin, Texas, Justin attended Texas A&M University at Galveston receiving a B.S. in Maritime Systems Engineering. Justin arrived at Texas A&M University in the fall of 2006, where he has worked under the supervision of Dr. Thomas Strganac.

Contact: Dr. Thomas Strganac; 3141 TAMU; College Station, TX 78743-3141

The typist for this thesis was Justin Patrick Jackson.